RESEARCH ARTICLE | OCTOBER 27 2023

Oblique collisions of three wet spheres ⊕⊘

Robert H. Davis 🕶 📵



Physics of Fluids 35, 103328 (2023) https://doi.org/10.1063/5.0171810







Physics of Fluids

Special Topic: Overview of Fundamental and Applied Research in Fluid Dynamics in UK

Submit Today





Oblique collisions of three wet spheres 🐵

Cite as: Phys. Fluids **35**, 103328 (2023); doi: 10.1063/5.0171810 Submitted: 10 August 2023 · Accepted: 8 October 2023 · Published Online: 27 October 2023









AFFILIATIONS

Department of Chemical and Biological Engineering, University of Colorado, Boulder, Colorado 80309-0596, USA

a) Author to whom correspondence should be addressed: robert.davis@colorado.edu

ABSTRACT

Oblique collisions of three solid spheres coated with thin viscous layers are simulated, both to elucidate the interesting physics of the collision outcomes and to lay the groundwork for a new approach to modeling flows of many wet particles. Included in the analysis are fluid viscous and capillary forces, as well as solid contact and friction forces. A novel approach is developed based on a rotating polar coordinate system for each particle pair in near contact, including the possibility that a given particle is in simultaneous contact with both other particles. As the Stokes number (a dimensionless ratio of particle inertia and viscous forces) is increased, the collision outcome progresses from full agglomeration (all three particles sticking together due to viscous and capillary forces) to partial agglomeration (two particles sticking together while the third one separates) to full separation (all three particles separating post-collision). The results are also sensitive to various physical and geometrical properties, such as the ratio of fluid film thickness to particle diameter, the coefficient of friction, and the collision angles.

Published under an exclusive license by AIP Publishing. https://doi.org/10.1063/5.0171810

I. INTRODUCTION

Dense flows of particles are prevalent in both nature (e.g., avalanches, mud slides, and river sediments) and in industry (e.g., pharmaceutical powders, paints, fracking media, agricultural grains and fertilizer pellets). It has been estimated that 50% of the world energy is derived from granular systems (Blumenfeld *et al.*, 2015) and that 75% of new materials in the chemical industry are in granular form (Nedderman, 1992).

Early theoretical and computational research on dense particulate processing primarily falls in two distinct categories: (i) dry granular flows, dominated by particle inertia and forces acting through particle-particle contacts, and (ii) wet suspension flows, in which fluid-particle forces dominate and particle interactions are mediated through the fluid, often with viscous forces dominating over inertia. The former may be described by the discrete element method (DEM) (Cundall and Strack, 1979), whereas the latter may be described by Stokesian dynamics (Brady and Bossis, 1988) and related methods.

More recent research has blended these two perspectives, such as gas—solid flows (e.g., gas fluidization) where particle inertia and particle-particle collision are still prevalent but drag forces on the particles by the gas phase are also key (Gidaspow, 1994). Another blended scenario is where the solid particles are not fully immersed in a liquid but rather are coated with thin layers of a viscous liquid such as in particle coating and agglomeration or de-agglomeration processes (Ennis et al., 1991; Guo and Curtis, 2015).

In recent years, the discrete element method (DEM) has been extended to wet or cohesive granular systems (Kantak et al., 2009; Anand et al., 2009; Radl et al., 2010; Liu et al., 2013; Umer and Siraj, 2018; Pähtz et al., 2019; Tang et al., 2019; and Kasper et al., 2021). These studies show that a small amount of liquid can drastically alter the behavior of granular flows (Liu et al., 2013; Pähtz et al., 2019). However, application of DEM to wet systems has proved challenging (Andreotti et al., 2013; Tang et al., 2019; and Kasper et al., 2021). In part, the difficulty is due to the relatively nascent understanding of the microscope nature of wet granular collisions, but it is also caused by challenges involved with time-step requirements and numerical stability (Washino et al., 2016). Moreover, most of the work has assumed that capillary forces dominate (Washino et al., 2013; Zhang and Li, 2017; Umer and Siraj, 2018; and Schmelzle and Nirschl, 2018), which is valid for fine powders with low-viscosity coatings like water. For larger particles with viscous coatings (polymers, oils, sirups, etc.), viscous lubrication forces will dominate except at very low collision velocities.

A key aspect of simulating flows of wet-particle systems is an accurate description of the fluid-mediated microphysical interaction of two wetted, colliding particles. Research on collisions of a wet solid particle with a surface or another particle was initiated nearly 40 years ago and sometimes referred to as "elastohydrodynamic collisions" (Davis *et al.*, 1986). The key concept is that there is a critical Stokes number, $St_n = mv_{n,0}/(6\pi\mu a^2)$, below which the particles stick due to

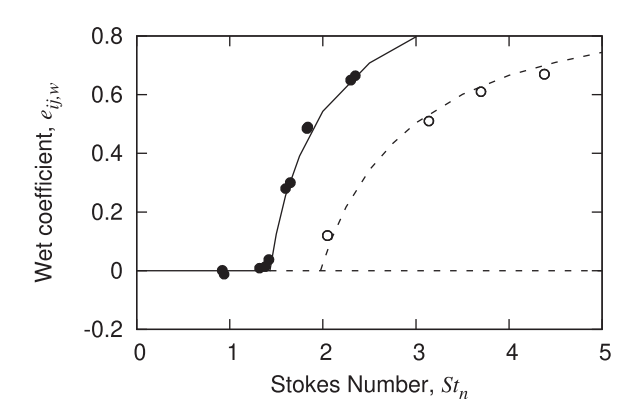


FIG. 1. Wet coefficient of restitution vs Stokes number for normal collisions of chrome steel spheres covered with a viscous oil $(\cdot,-)$ and of stainless-steel spheres covered with a less viscous oil $(\cdot,-)$. The symbols are experimental data from Donahue *et al.* (2012), and the curves are the model predictions of Davis and Sitison (2020).

viscous losses and above which they bounce with a reduced coefficient of restitution (as some of their initial kinetic energy is lost to viscous dissipation)—see Fig. 1. Here, m and a are the reduced mass and radius, respectively, of the two colliding objects, $v_{n,0}$ is their initial relative velocity in the direction normal to their surfaces, and μ is the fluid viscosity.

Subsequent research on the microphysics of wet-particle collisions has included both fully immersed collisions (Davis, 1987; Gondret et al., 1999; Joseph et al., 2001; Lian et al., 1996; and Yang and Hunt, 2006) and collisions involving thin liquid layers (Barnocky and Davis, 1988; Davis et al., 2002; Donahue et al., 2012; Gollwitzer et al., 2012; Ma et al., 2013; Crüger et al., 2016; Buck et al., 2018; and Danczyk et al., 2022). Müller and Huang (2016) used an energy model to examine the conversion of kinetic energy to viscous dissipation, fluid inertia, and contact losses. They demonstrated that a plot of the wet coefficient of restitution vs inverse Stokes number yields a straight line, as predicted by Barnocky and Davis (1988). While initial research focused on normal or head-on collisions, recent studies have included oblique collisions (Kantak and Davis, 2004, 2006; Joseph and Hunt, 2004; Donahue et al., 2012; Sutkar et al., 2015; Buck et al., 2017; Davis and Sitison, 2020; and Punch et al., 2023). For particle collisions with a flat, wetted surface, key findings include that the normal motion is nearly unaffected by the tangential motion and that the sliding lubrication resistance to tangential motion is relatively small, though the latter

can impact sphere rotation and reduce dry friction (Kantak and Davis, 2006; Ma et al., 2013; and Buck et al., 2017). A nice review of modeling approaches and comparison with experiments is provided by Buck and Heinrich (2019). Oblique collisions of two wetted spheres have relatively rich physics (Fig. 2), including sticking or agglomeration at low Stokes numbers, rapid bouncing at high Stokes numbers, and a stick-rotate-separate phenomenon at intermediate Stokes numbers, where the two spheres initially stick together due to viscous losses, rotate as a doublet due to conservation of angular momentum, and then slowly separate due to centrifugal forces if the capillary suction in the pendant liquid bridge is not sufficiently strong (Donahue et al., 2012; Davis and Sitison, 2020).

This paper provides a theoretical examination of the microphysics and outcomes of oblique collisions involving three wetted particles. While an extension to three-particle collisions may seem to be a small step beyond two-particle collisions, the possible outcomes are relatively rich, including full-agglomeration (FA), where all three spheres stick together, partial agglomeration (PA), where two spheres stick together and the third one (which can be any of the three spheres, depending on the conditions) separates, and full separation (FS), where all three spheres separate after the collision. Moreover, the dynamics are complicated by the possibility of a sphere being in simultaneous contact with more than one neighboring spheres, and developing the tools to handle this situation is a key step in designing a new DEM approach for flows of many wet particles. To our knowledge, microphysical simulations and experiments with a few (e.g., 3-5) wet spheres are largely absent from the literature, with exceptions including the special case of colinear configurations (Donahue et al., 2010; Davis, 2019) and DEM simulations of a cohesive singlet colliding with an agglomerated doublet (Liu et al., 2017). In what follows, the problem formulation is first presented in general terms for an unspecified number N spheres, with each sphere potentially in close contact with multiple neighboring spheres. Newton's laws of motion are recast in a rotating polar coordinate system for each pair of interacting spheres. Next, the governing equations for the special case of three equal spheres are presented, followed by results and discussion and then concluding remarks.

II. GENERAL PROBLEM FORMULATION

We initially consider the general case of N spheres of radius a_i (i=1,2,...,N), each coated with a thin viscous fluid of viscosity μ and thickness $\delta_i \ll a_i$ and having mass m_i (neglecting the thin film). Newton's laws of motion for each sphere i are

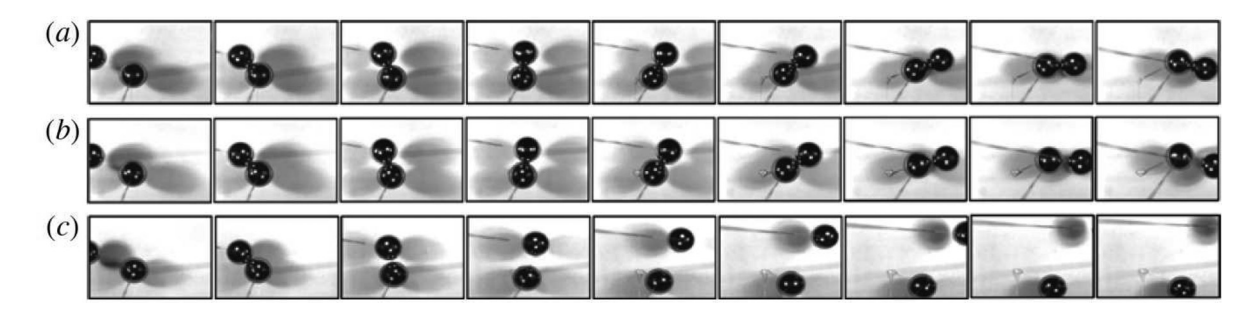


FIG. 2. Illustration of collisions of two wet spheres with outcomes of (a) sticking with $St_n = 0.95$, (b) stick-rotate-separate with $St_n = 1.1$, and (c) bounce with $St_n = 1.3$. Figure reprinted with permission from Donahue *et al.*, J. Fluid Mech. **708**, 128–148 (2012). Copyright 2012 Cambridge University Press.

$$m_i d\mathbf{v}_i / dt = -\sum \mathbf{F}_{ik} + m_i \mathbf{g}, \qquad (1)$$

$$d\mathbf{x}_i/dt = \mathbf{v}_i, \quad i = 1, 2, ...N, \tag{2}$$

where v_i is the translational velocity of the center of sphere i, located at x_i , g is the gravitational acceleration, and $-F_{ik} = +F_{ki}$ is the hydrodynamic force acting on sphere i via the thin fluid film between spheres i and k. The sum is over all spheres that are in close contact (i.e., having overlapped liquid layers) with sphere i.

An illustration for the special case of three equal spheres is shown in Fig. 3. For simplicity, the motion is confined to a plane formed by the centers of the three spheres. It is further assumed that the only forces exerted on the spheres are gravity plus viscous lubrication and capillary forces from overlapping liquid layers when two spheres are nearly touching; any drag forces from the surrounding air are neglected. Figure 3 shows the initial configuration at time t = 0, when the striker sphere (sphere 1) first collides with a target sphere (sphere 2), which is already agglomerated with the third sphere. The collision interaction begins when the films on spheres 1 and 2 first overlap. At t = 0, the 2-3 doublet is assumed stationary, whereas sphere 1 has velocity of magnitude $v_{1,0}$ and moves at an angle α from the x-axis. Also shown are polar coordinates, defined such that r_{ii} is the distance from the center of the sphere *i* to the center of sphere *j* and θ_{ii} is the angle from the x-axis to the line-of-centers of spheres i and j. Note that the polar coordinate system for each particle pair will rotate with time, whereas the Cartesian coordinates are fixed.

The hydrodynamic forces in (1) are due to viscous lubrication and capillary forces exerted by the thin film between an *i*–*j* pair of particles and may be decomposed into normal (along the line-of-centers) and tangential (perpendicular to the line-of-centers) components (Davis and Sitison, 2020)

$$F_{ij,n} = 6\pi \mu a_{ij}^2 v_{ij,n} \left[1 - h_{ij} / (2\delta_{ij} - h_{ij}) \right]^2 / h_{ij} - 8\pi a_{ij} \sigma, \tag{3}$$

$$F_{ij,t} = 2\pi \mu a_{ij} v_{ii,t}^s \ln[(2\delta_{ij} - h_{ij})/h_{ij}], \tag{4}$$

where μ is the liquid viscosity, σ is the interfacial tension of the liquid, $a_{ij}=a_ia_j/(a_i+a_j)$ is the reduced radius, $v_{ij,n}=v_{i,n_{ij}}-v_{j,n_{ij}}$ is the relative velocity along the line-of-centers, $h_{ij}=r_{ij}-a_i-a_j$ is the closest distance separating the two surfaces, $\delta_{ij}=\delta_i+\delta_j$ is the separation distance when the adjacent liquid layers first begin to overlap, and $v_{ij,t}^s=v_{i,t_{ij}}^s-v_{j,t_{ij}}^s=-r_{ij}\Omega_{ij}+\omega_ia_i+\omega_ja_j$ is the relative velocity of the sphere surfaces in the tangential direction (see Fig. 4). Here, r_{ij} is the center-to-center distance, $\Omega_{ij}=d\theta_{ij}/dt$ is the rate of rotation of the line-of-centers, and ω_i and ω_j are the rotational velocities of the

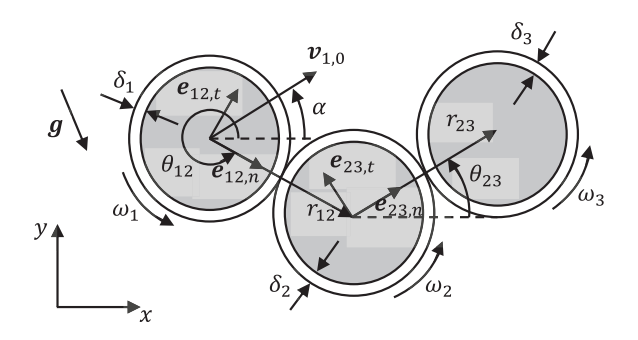


FIG. 3. Defining sketch for three colliding spheres.

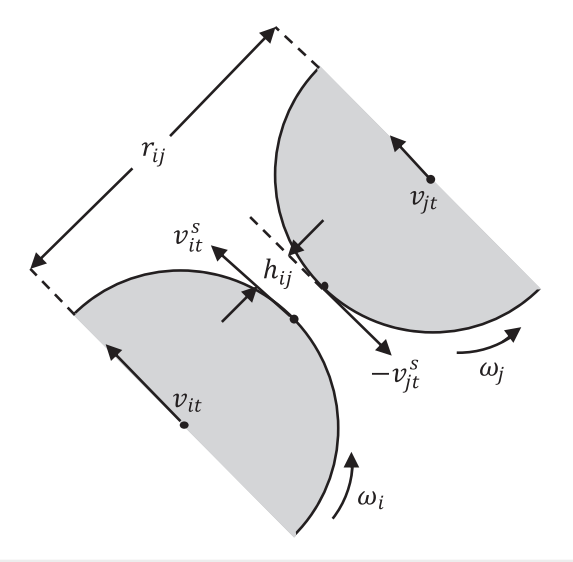


FIG. 4. Tangential and rotational velocities of the i–j pair of spheres in near contact (liquid films not shown).

individual spheres (all defined to be positive for counterclockwise rotation). The first term on the right-hand-side of (3) is the viscous force that resists relative motion in the normal direction, derived from the Reynolds lubrication equation with a thin film of finite extent. The term in brackets corresponds to a correction due to the finite radial extent of the film between the two curved surfaces in near contact [see Fig. 2 of Davis and Sitison (2020)]. Danczyk et al. (2022) compared various models with experimental results for colinear collisions and concluded that inclusion of such a correction factor gave better agreement than use of the traditional viscous lubrication force between fully immersed surfaces. Equation (3) also applies for aspherical particles, which are gaining increased attention (Guo and Curtis, 2015), provided that their local surfaces in the region of near contact can be fitted by paraboloids—a modification would be required if the surface curvatures differ in two orthogonal directions. Note that the viscous term becomes negative (a suction force) when the spheres are moving apart. Cavitation is a possibility when a negative suction pressure occurs, which would limit the suction force, but prior analysis of experiments (Donahue et al., 2010, 2012) inferred that the full suction force remained in effect (perhaps due to the short timescale and high viscosity limiting the formation of cavitation bubbles). It is assumed that the Reynolds number $Re = \rho v_{ij,n} \delta_{ij} / \mu$ (with ρ being the fluid density) is small for thin gaps, so fluid inertia is negligible. The second term on the right-hand-side of (3) is the capillary suction force in the thin liquid bridge between the two spheres (Davis and Sitison, 2020). Equation (4) comes from integrating the shear stress due to sliding motion over the extent of the thin film where the two spheres are in near contact (Kantak and Davis, 2006; Davis and Sitison, 2020). Both expressions assume that the film has axial symmetry about the line-of-centers, though it may be that the tangential motion causes the film to become distorted.

A. Normal component of translational motion

Since the hydrodynamic forces depend on the relative velocity between the two spheres, decomposed into motion along the line-ofcenters (normal to the surfaces) and perpendicular to the line-ofcenters (tangential to the surfaces), we recast the governing equations into a unique polar coordinate system for each i–j pair. Rotating polar coordinates have been used for both dry and wet collisions involving just two spheres (Müller and Pöschel, 2012; Donahue *et al.*, 2012; and Davis and Sitison, 2020), although works considering multibody collisions generally use Cartesian coordinates. Starting with the normal component for sphere i in the direction along the line-of-centers with sphere j, the product rule and geometry yield

$$\mathbf{e}_{ij,n} \cdot d\mathbf{v}_i / dt = d(\mathbf{e}_{ij,n} \cdot \mathbf{v}_i) / dt - \mathbf{v}_i \cdot d\mathbf{e}_{ij,n} / dt$$

$$= d\mathbf{v}_{i,n,i} / dt - \mathbf{v}_{i,t,i} d\theta_{ij} / dt, \tag{5}$$

where $e_{ij,n}$ is the unit vector in the r_{ij} direction (i.e., along the line-of-centers from sphere i to sphere j). Furthermore, $e_{ij,n} \cdot F_{ij} = F_{ij,n}$ is the normal component of the hydrodynamic force between spheres i and j, as given in (3). For any other sphere in contact with sphere i, a simple geometric analysis is needed to determine the hydrodynamic force in the $e_{ij,n}$ direction,

$$\mathbf{e}_{ij,n} \cdot \mathbf{F}_{ik} = F_{ik,n} \cos(\theta_{ik} - \theta_{ij}) - F_{ik,t} \sin(\theta_{ik} - \theta_{ij}), \tag{6}$$

where $F_{ik,n}$ is in the direction of increasing r_{ik} (i.e., parallel to the i–k line-of-centers) and $F_{ik,t}$ is in the direction of increasing θ_{ik} , (i.e., perpendicular to the i–k line-of-centers). Thus, the normal component of (1) becomes

$$m_{i}dv_{i,n_{ij}}/dt = m_{i}v_{i,t_{ij}}d\theta_{ij}/dt - F_{ij,n}$$

$$-\sum_{i} \left[F_{ik,n}\cos\left(\theta_{ik} - \theta_{ij}\right) - F_{ik,t}\sin(\theta_{ik} - \theta_{ij})\right]$$

$$+ m_{i}(g_{x}\cos\theta_{ij} + g_{y}\sin\theta_{ij}), \tag{7}$$

where the sum is over all spheres k except sphere j in close contact with sphere i. A similar expression applies for the normal component of the motion of sphere j,

$$m_{j}dv_{j,n_{ij}}/dt = m_{j}v_{j,t_{ij}}d\theta_{ij}/dt + F_{ij,n}$$

$$-\sum_{i} \left[F_{jl,n}\cos(\theta_{jl} - \theta_{ij}) - F_{jl,t}\sin(\theta_{jl} - \theta_{ij})\right]$$

$$+ m_{j}(g_{x}\cos\theta_{ij} + g_{y}\sin\theta_{ij}), \tag{8}$$

which comes from (7) with the indices i and j swapped and the following identities: $\theta_{ji} = \theta_{ij} + \pi$, $F_{ji,n} = F_{ij,n}$, $v_{j,n_{ji}} = -v_{j,n_{ij}}$, and $v_{j,t_{ji}} = -v_{j,t_{ij}}$; in addition, the sum is over all spheres l except sphere i in contact with sphere i.

The relative normal velocity of the i–j pair along its line-of-centers, $v_{ij,n} = v_{i,n_{ij}} - v_{j,n_{ij}}$, is then found by multiplying (8) by m_i and subtracting it from (7) multiplied by m_{j} , yielding

$$m_{ij}dv_{ij,n}/dt = -m_{ij}r_{ij}\Omega_{ij}^{2} - F_{ij,n}$$

$$-m_{j} \sum_{i} \left[F_{ik,n}\cos\left(\theta_{ik} - \theta_{ij}\right) - F_{ik,t}\sin\left(\theta_{ik} - \theta_{ij}\right)\right]/(m_{i} + m_{j})$$

$$+m_{i} \sum_{i} \left[F_{jl,n}\cos\left(\theta_{jl} - \theta_{ij}\right) - F_{il,t}\sin\left(\theta_{il} - \theta_{ij}\right)\right]/(m_{i} + m_{i}), \tag{9}$$

where $v_{ij,t}=v_{i,t_{ij}}-v_{j,t_{ij}}=-r_{ij}d\theta_{ij}/dt$ is the relative tangential velocity and $m_{ij}=m_im_j/(m_i+m_j)$ is the reduced mass. The definition $\Omega_{ij}=d\theta_{ij}/dt$ as the rate of rotation of the line-of-centers has also been employed.

B. Tangential component of translational motion

For the tangential component of the motion of sphere i, which is in the direction perpendicular to the line-of-centers with sphere j,

$$\begin{aligned} \mathbf{e}_{ij,t} \cdot d\mathbf{v}_i / dt &= d(\mathbf{e}_{ij,t} \cdot \mathbf{v}_i) / dt - \mathbf{v}_i \cdot d\mathbf{e}_{ij,t} / dt \\ &= d\mathbf{v}_{i,t_{ij}} / dt + \mathbf{v}_{i,n_{ij}} d\theta_{ij} / dt, \end{aligned} \tag{10}$$

where $e_{ij,t}$ is the unit vector in the direction of increasing θ_{ij} (i.e., tangent to the interface and normal to the line-of-centers). Furthermore, $e_{ij,t} \cdot F_{ij} = F_{ij,t}$ is the tangential component of the hydrodynamic force between spheres i and j. For another sphere in close contact with sphere i,

$$\mathbf{e}_{ij,t} \cdot \mathbf{F}_{ik} = -F_{ik,n} \sin \left(\theta_{ik} - \theta_{ij}\right) - F_{ik,t} \cos(\theta_{ik} - \theta_{ij}) . \tag{11}$$

Thus, the tangential component of (1) for sphere i becomes

$$m_{i}dv_{i,t_{ij}}/dt = -m_{i}v_{i,n_{ij}}d\theta_{ij}/dt - F_{ij,t}$$

$$-\sum_{i} \left[F_{ik,n}\sin\left(\theta_{ik} - \theta_{ij}\right) + F_{ik,t}\cos\left(\theta_{ik} - \theta_{ij}\right)\right]$$

$$+ m_{i}(g_{x}\sin\theta_{ij} + g_{y}\cos\theta_{ij}), \tag{12}$$

where again the sum is over all spheres except sphere j that are in close contact with sphere i. A similar expression applies for the tangential component of the motion of sphere j,

$$m_{j}dv_{j,t_{ij}}/dt = -m_{j}v_{j,n_{ij}}d\theta_{ij}/dt + F_{ij,t}$$

$$+ \sum_{l} \left[F_{jl,n}\sin\left(\theta_{jl} - \theta_{ij}\right) + F_{jl,t}\cos\left(\theta_{jl} - \theta_{ij}\right) \right]$$

$$+ m_{i}(g_{x}\sin\theta_{ii} + g_{y}\cos\theta_{ii}),$$

$$(13)$$

using the previous identities along with $F_{jl,t} = F_{lj,t}$.

The relative tangential velocity, $v_{ij,t} = v_{i,t_{ij}} - v_{j,t_{ij}}$, is then found by multiplying (13) by m_i and subtracting it from (12) multiplied by m_i ,

$$\begin{split} m_{ij} \left[r_{ij} d\Omega_{ij} / dt + \Omega_{ij} dh_{ij} / dt \right] \\ &= m_{ij} v_{ij,n} \Omega_{ij} + F_{ij,t} + m_j \sum_{j} \left[F_{ik,n} \sin \left(\theta_{ik} - \theta_{ij} \right) + F_{ik,t} \cos \left(\theta_{ik} - \theta_{ij} \right) \right] / \left(m_i + m_j \right) \\ &- m_i \sum_{j} \left[F_{jl,n} \sin \left(\theta_{jl} - \theta_{ij} \right) + F_{jl,t} \cos \left(\theta_{jl} - \theta_{ij} \right) \right] / \left(m_i + m_j \right). \end{split}$$

Here, $v_{ij,t} = -r_{ij}d\theta_{ij}/dt$, $r_{ij} = h_{ij} + a_i + a_j$, and $\Omega_{ij} = d\theta_{ij}/dt$ have been employed.

C. Rotational motion

Taking the cross product of the position vector (measured from the center of mass) and integrating over all positions within sphere i yield

$$I_i d\omega_i / dt = -\sum T_{ik}, \qquad (15)$$

where $-T_{ik} = r \times (-F_{ik})$ is the torque exerted by sphere k on sphere i. Note that gravity acts through the center of mass and does not contribute to the torque, with the same true of the normal forces acting along the line-of-centers. The moment of inertia of a solid sphere i with uniform density is $I_i = 2m_i a_i^2/5$, neglecting the thin fluid layer.

The torque exerted by sphere k on sphere i is a pseudo-vector in the z-direction (out of the plane shown in Fig. 3), as are the angular velocities, with z-component $T_{ik} = a_i F_{ik,t}$. Thus, (15) becomes

$$I_i d\omega_i / dt = -\sum a_i F_{ik,t}. \tag{16}$$

Since $v_{ij,t}^s = -r_{ij}\Omega_{ij} + \omega_i a_i + \omega_j a_j$ is needed in (4) for the tangential lubrication force, we define $v_{ij,\omega} = \omega_i a_i + \omega_j a_j$. Then, multiplying by (16) by $I_j a_i$ and adding it to a similar expression for sphere j multiplied by $I_i a_j$ yield

$$I_{i}I_{j}dv_{ij,\omega}/dt = -\left(I_{j}a_{i}^{2} + I_{i}a_{j}^{2}\right)F_{ij,t} - I_{j}a_{i}^{2}\sum F_{ik,t} - I_{i}a_{j}^{2}\sum F_{jl,t},$$
(17)

where the first sum is over all spheres k except sphere j in contact with sphere i, and the second sum is over all spheres l except sphere i in contact with sphere j.

D. Equation summary and general approach

For each i–j particle pair in near contact, there are five dependent variables associated with the relative motion of that pair: surface separation h_{ij} line-of-centers angle θ_{ij} , relative normal velocity along the line-of-centers $v_{ij,n}$, angular velocity of the line-of-centers Ω_{ij} , and the relative surface velocity due to sphere rotation $v_{ij,\omega}$. They are governed by the first-order ordinary differential equations (9), (14), and (17), plus the two kinematic conditions

$$dh_{ii}/dt = -v_{ii,n}, \quad d\theta_{ii}/dt = \Omega_{ii}.$$
 (18)

The required hydrodynamic forces are given in (3) and (4), with $v_{ii,t}^s = -r_{ij}\Omega_{ij} + v_{ij,\omega}$, where $r_{ij} = a_i + a_j + h_{ij}$. The resulting system of nonlinear, first-order ordinary differential equations for particle pairs in near contact, along with initial conditions for the particle positions and velocities, may be solved by Runge-Kutta or other standard numerical methods for initial-value problems. There may also be analytical or semi-analytical approximate solutions for limiting cases, such as demonstrated by Davis (2019) for three spheres in a line and by Davis and Sitison (2020) for fast and slow oblique collisions of two spheres. Although the governing equations in the pairwise rotating polar coordinate systems are more complex than the original governing equations in fixed Cartesian coordinates for the translational and rotational velocities of each sphere, the present approach is expected to have two significant advantages: (i) the necessary force expressions are already resolved into their natural components along and normal to the line of centers and contain the pairwise relative velocities directly computed in the solution, whereas using Cartesian coordinates for each sphere would require computing the relative velocities and then decomposing the force expressions into x and y components at each time step, and (ii) the pairwise approach will accurately resolve the small relative velocities and surface separations along the line-of-centers (as they are direct variables in the simulations), whereas small but accumulating errors in the absolute velocities and positions for the individual-sphere approach in Cartesian coordinates could yield significant errors when the differences in positions and velocities are computed, requiring high resolution and small time steps.

E. Solid-solid contact and velocity reversal

If the sphere surfaces are perfectly smooth and the fluid is treated as a continuum without molecular effects (such as slip or attractions), then the viscous lubrication layer will prevent solidsolid contact, because the resisting lubrication force in (3) becomes singular as the gap approaches zero. However, prior work by our group (Davis et al., 1986; Davis, 1987; Barnocky and Davis, 1988, 1989; Donahue et al., 2010, 2012; Davis, 2019; and Davis and Sitison, 2020) has described at least three scenarios where solid-like contact and subsequent rebound can occur when the gap becomes sufficiently small (typically on the order of micrometers): (i) glass transition of the liquid due to high lubrication pressure, (ii) elastohydrodynamic deformation of the solids, also due to high lubrication pressure, and (iii) solid-solid contact due to particle surface roughness. For pendulum experiments using smooth metal balls and very viscous liquid coatings, the glass-transition mechanism has been found to dominate (Donahue et al., 2010, 2012; Danczyk et al., 2022; and Punch et al., 2023). However, for natural systems with larger surface roughness and lower viscosity of the film (e.g., water), surface roughness may dominate, while elastohydrodynamic deformation may be most important for soft particles.

Once solid-solid or solid-like [here, "solid-like" might include scenarios (i) and (ii) above, where the two particles do not come into physical contact but still store and release energy due to elastic deformation caused by high lubrication pressures contact occurs, then this contact may be treated either as a hard-sphere collision or a softsphere collision. For a hard-sphere collision, the solid-like contact is assumed to be instantaneous, resulting in an impulse with a normal component (i.e., along the line-of-centers) that causes the normal component of the relative velocity to reverse sign and typically be multiplied by e_{dry} (a dry coefficient of restitution, accounting for energy loss due to inelastic effects as the solids deform and release). There may also be changes in tangential and rotational motion during the reversal of the normal velocity, due to friction, as previously described by considering a tangential impulse equal to the normal impulse multiplied by a coefficient of friction (Davis and Sitison, 2020). In contrast, a soft-sphere collision is enduring, taking place over multiple time steps and using the Hertzian contact theory or a spring-dashpot model for the solid deformation and a friction model for solid-solid tangential forces.

Stratton and Wensrich (2010) and Müller and Pöschel (2012) and others have investigated the advantages and limitations of the hard-sphere model for dry collisions. For wet collisions, Davis (2019) estimated the characteristic time for solid-solid contact from Hertzian contact theory and found that it is two orders-of-magnitude smaller than the characteristic time for penetration through the viscous fluid coating for the experiments of Donahue et al. (2010), thus justifying the use of a hard-sphere model with essentially instantaneous contact and velocity reversal. These experiments used stiff materials (steel spheres) with relative high impact velocities $(\sim 1 \text{ m/s})$ and thick fluid coatings $(\sim 0.1-1 \text{ mm})$. Softer materials and thinner coatings would increase the ratio of solid-solid contact time and fluid-penetration time, thereby pointing toward the need for a soft-sphere model for the solid-contact phase. In the current work, a soft-sphere (non-instantaneous) model is used for the penetration through the liquid film, but a hard-sphere (instantaneous) model is employed for solid-like contact. An extension to a softsphere model for both stages would be straightforward. The details of the "jump" in velocities when a hard-sphere collision occurs are lengthy and given in Appendix A.

III. SPECIAL CASE OF THREE EQUAL SPHERES

We focus the rest of the paper on the special case of three equal spheres, with $m_i = 2m$, $a_i = 2a$, and $I_i = 16ma^2/5$ for i = 1, 2, and 3, where m is the reduced mass and a is the reduced radius. The spheres are numbered such that sphere 2 is the middle or "target" sphere, as shown in Fig. 3. Sphere 1 is the "striker" sphere, which collides with sphere 2, while sphere 3 is initially on the other side of sphere 2. We consider the event-driven problem where spheres 2 and 3 are initially at rest and separated by a gap $h_{23,0}$, and then at t=0sphere 1 collides with sphere 2 with velocity of magnitude $v_{1,0}$ and angle α from the x axis (measured in the counterclockwise direction, as shown in Fig. 3). To keep the number of variables modest, it is assumed that none of the spheres are rotating before the collision. The initial conditions are then $h_{12} = h_{12,0} = \delta_{12}, h_{23} = h_{23,0}, \theta_{12} = \theta_{12,0},$ $\theta_{23} = \theta_{23,0}, \ v_{12,n} = v_{1,0}\cos(\alpha - \theta_{12,0}), \ v_{23,n} = 0, \ \Omega_{12} = -v_1^0\sin(\alpha - \theta_{12,0})$ $-\theta_{12,0})/4a$, and $\Omega_{23}=\omega_{12}=\omega_{23}=0$ at t=0, where $\omega_{ij}=\omega_i+\omega_j$. Note that $h_{12,0} = \delta_{12} = \delta_1 + \delta_2$ by definition (since t = 0 is defined as when the liquid layers on the 1–2 pair first overlap), but $h_{23,0}$ is not necessarily equal to $\delta_{23} = \delta_2 + \delta_3$ (since we allow for the possibility that the 2-3 pair is not initially in contact or that their films are already overlapping). As described previously (Davis and Sitison, 2020), oblique collisions of two (or more) wet spheres have two (or more) timescales. First, there is a short timescale, $t_S = \delta_{12}/(v_{1,0}\cos\beta)$, where $\beta = \alpha - \theta_{12.0}$ and $v_{1.0} \cos \beta$ is the normal component of the initial relative impact velocity of this pair. Thus, t_S is a measure of time required for sphere 1 to penetrate through the thin liquid layer separating it from sphere 2, if it has enough inertia to overcome the viscous lubrication resistance and maintain its velocity. Second, there is a long timescale, $t_L = 4a/(v_{1,0}\sin\beta)$, where $v_{1,0}\sin\beta$ is the tangential component of the initial relative impact velocity. Thus, t_L is a measure of the time required for an agglomerated pair of particles to rotate one radian, if the collision did not have enough inertia for them to rapidly bounce apart. The ratio of the two time scales is $t_L/t_S = 4a/$ $(\delta_{12} \tan \beta)$, which is large compared to unity for thin films $(\delta_{12}/4a \ll 1)$, except for glancing collisions for which $\beta \approx \pi/2$. As discussed by Davis (2019), there is also a very short timescale, $t_C = (\rho_s^2 \theta^2 a^5 / v_{1,0} \cos \beta)^{1/5}$ associated with the Hertzian solid-solid contact, where ρ_s is the solid density and $\theta = 2(1 - \nu^2)/\pi E$, with ν being Poisson's ratio and E Young's modulus, of the colliding spheres. As noted previously, $t_C \ll t_S$, except for very thin films and soft particles.

Following Davis and Sitison (2020) for oblique collisions of two wet spheres, the short timescale (t_S) and initial separation (δ_{12}) are chosen for the following dimensionless variables:

$$\hat{t} = v_{n,0}t/\delta_{12}, \quad \hat{h}_{ij} = h_{ij}/\delta_{12}, \quad \hat{v}_{ij,n} = v_{ij,n}/v_{n,0}, \hat{\Omega}_{ij} = \Omega_{ij}4a/v_{t,0}, \quad \hat{\omega}_{ij} = \omega_{ij}4a/v_{t,0},$$
(19)

where $v_{n,0}=v_{1,0}\cos{(\alpha-\theta_{12,0})}$ and $v_{t,0}=v_{1,0}\sin{(\alpha-\theta_{12,0})}$ are the initial normal and tangential relative velocities, respectively, for the 1–2 pair. It is noted that, without loss of generality, the x-y coordinate system can be defined such that $\alpha=0$ or $\theta_{12,0}=0$. The governing system of non-dimensional equations for three equal spheres is

$$St_{n}d\hat{v}_{12,n}/d\hat{t} = -St_{n}(\tan\beta)^{2}\hat{h}_{a}\hat{r}_{12}\hat{\Omega}_{12}^{2} - \hat{F}_{12,n}$$

$$- \left[\hat{F}_{13,n}\cos(\theta_{13} - \theta_{12}) - \hat{F}_{13,t}\sin(\theta_{13} - \theta_{12})\right]/2$$

$$+ \left[\hat{F}_{23,n}\cos(\theta_{23} - \theta_{12}) - \hat{F}_{23,t}\sin(\theta_{23} - \theta_{12})\right]/2,$$
(20)

$$St_{n}\hat{r}_{12}d\hat{\Omega}_{12}/d\hat{t} = 2St_{n}\hat{h}_{a}\hat{v}_{12,n}\hat{\Omega}_{12} + \hat{F}_{12,t}\cot\beta$$

$$+ \left[\hat{F}_{13,n}\sin(\theta_{13} - \theta_{12}) + \hat{F}_{13,t}\cos(\theta_{13} - \theta_{12})\right](\cot\beta)/2$$

$$- \left[\hat{F}_{23,n}\sin(\theta_{23} - \theta_{12}) + \hat{F}_{23,t}\cos(\theta_{23} - \theta_{12})\right](\cot\beta)/2, \qquad (21)$$

$$St_n d\hat{\omega}_{12}/d\hat{t} = -5(\hat{F}_{12,t} + \hat{F}_{13,t}/2 + \hat{F}_{23,t}/2)\cot\beta,$$
 (22)

$$St_{n}d\hat{v}_{23,n}/d\hat{t} = -St_{n}(\tan\beta)^{2}\hat{h}_{a}\hat{r}_{23}\hat{\Omega}_{23}^{2} - \hat{F}_{23,n}$$

$$- \left[\hat{F}_{13,n}\cos(\theta_{13} - \theta_{23}) - \hat{F}_{13,t}\sin(\theta_{13} - \theta_{23})\right]/2$$

$$+ \left[\hat{F}_{12,n}\cos(\theta_{23} - \theta_{12}) + \hat{F}_{12,t}\sin(\theta_{23} - \theta_{12})\right]/2,$$
(23)

$$St_{n}\hat{r}_{23}d\hat{\Omega}_{23}/d\hat{t} = 2St_{n}\hat{h}_{a}\hat{v}_{23,n}\hat{\Omega}_{23} + \hat{F}_{23,t}\cot\beta$$

$$+ \left[\hat{F}_{13,n}\sin(\theta_{13} - \theta_{23}) + \hat{F}_{13,t}\cos(\theta_{13} - \theta_{23})\right](\cot\beta)/2$$

$$+ \left[\hat{F}_{12,n}\sin(\theta_{23} - \theta_{12}) - \hat{F}_{12,t}\cos(\theta_{23} - \theta_{12})\right](\cot\beta)/2, \tag{24}$$

$$St_n d\hat{\omega}_{23}/d\hat{t} = -5(\hat{F}_{23,t} + \hat{F}_{13,t}/2 + \hat{F}_{12,t}/2)\cot\beta,$$
 (25)

$$d\hat{h}_{12}/d\hat{t} = -\hat{v}_{12,n}, d\theta_{12}/d\hat{t} = \hat{h}_a(\tan\beta)\hat{\Omega}_{12}, \tag{26}$$

$$d\hat{h}_{23}/d\hat{t} = -\hat{v}_{23,n}, d\theta_{23}/d\hat{t} = \hat{h}_a(\tan\beta)\hat{\Omega}_{23},$$
 (27)

where $\hat{h}_a = \delta_{12}/4a$ is the dimensionless film thickness, $\beta = \alpha - \theta_{12,0}$ is the impact angle, $\hat{r}_{ij} = r_{ij}/4a$, and $St_n = mv_{n,0}/6\pi\mu a^2$ is the Stokes number based on the normal component of the impact velocity and represents the ratio of particle inertia and the viscous fluid force. Note that these equations include the possibility that sphere 1 may interact with both spheres 2 and 3, which would occur if it rotated around sphere 2 and eventually encountered sphere 3 (see Sec. V). The corresponding dimensionless forces from the thin fluid films between the pairs are

$$\hat{F}_{12,n} = \hat{v}_{12,n} \left[1 - \hat{h}_{12} / (2 - \hat{h}_{12}) \right]^2 / \hat{h}_{12} - 4 / Ca, \tag{28}$$

$$\hat{F}_{13,n} = \hat{v}_{13,n} \left[1 - \hat{h}_{13} / (2\hat{d}_{13} - \hat{h}_{13}) \right]^2 / \hat{h}_{13} - 4/Ca, \tag{29}$$

$$\hat{F}_{23,n} = \hat{v}_{23,n} \left[1 - \hat{h}_{23} / (2\hat{d}_{23} - \hat{h}_{23}) \right]^2 / \hat{h}_{23} - 4 / Ca,$$
 (30)

$$\hat{F}_{12,t} = \left(\frac{h_{12,0}}{3a}\right) \tan \beta \left[-\hat{r}_{12}\hat{\Omega}_{12} + \frac{\hat{\omega}_{12}}{2} \right] \ln \left[\frac{\left(2 - \hat{h}_{12}\right)}{\hat{h}_{12}} \right], \quad (31)$$

$$\hat{F}_{13,t} = \left(\frac{h_{12,0}}{3a}\right) \tan \beta \left[-\hat{r}_{13}\hat{\Omega}_{13} + \frac{\hat{\omega}_{13}}{2} \right] \ln \left[\frac{(2\hat{d}_{13} - \hat{h}_{13})}{\hat{h}_{13}} \right], \quad (32)$$

$$\hat{F}_{23,t} = \left(\frac{h_{12,0}}{3a}\right) \tan \beta \left[-\hat{r}_{23}\hat{\Omega}_{23} + \frac{\hat{\omega}_{23}}{2} \right] \ln \left[\frac{(2\hat{d}_{23} - \hat{h}_{23})}{\hat{h}_{23}} \right], \quad (33)$$

where $\hat{F} = F/(6\pi\mu a^2 v_{n,0}/\delta_{12})$, $\hat{d}_{23} = \delta_{23}/\delta_{12}$, $\hat{d}_{13} = \delta_{13}/\delta_{12}$, and $Ca = 3\mu a v_{n,0}/(\delta_{12}\sigma)$ is the capillary number and represents the ratio

of viscous forces and interfacial forces. Note, however, that the fluid forces in (28)–(33) become zero when the liquid layers do not overlap: $\hat{h}_{12} > 1$ for the 1–2 pair, $\hat{h}_{13} > \hat{d}_{13}$ for the 1–3 pair, and $\hat{h}_{23} > \hat{d}_{23}$ for the 2–3 pair; in this case, the capillary bridge is expected to break or else have negligible influence when the sphere surfaces separate beyond the sum of their film thicknesses. Finally, the initial conditions for the dimensionless variables are $\hat{h}_{12} = 1$, $\hat{h}_{23} = h_{23,0}/\delta_{12}$, $\theta_{12} = \theta_{12,0}$, $\theta_{23} = \theta_{23,0}$, $\hat{v}_{12,n} = 1$, $\hat{v}_{23,n} = 0$, $\hat{\Omega}_{12} = -1$, and $\hat{\Omega}_{23} = \hat{\omega}_{12} = \hat{\omega}_{23} = 0$ at $\hat{t} = 0$

The above equations describe the dynamics of the relative motion of each particle pair in near contact. In many applications, it may be desirable to track each particle individually in a fixed coordinate system. The current method may still be employed, by solving the laws of motion to follow one particle and then tracking the remaining particles in using the relative motion. Choosing sphere 1 as the first particle to track, the x and y components of (1) and (2) in non-dimensional form are

$$2St_n d\hat{v}_{1,x}/d\hat{t} = -\hat{F}_{12,n}\cos\theta_{12} + \hat{F}_{12,t}\sin\theta_{12} - \hat{F}_{13,n}\cos\theta_{13} + \hat{F}_{13,t}\sin\theta_{13} + \hat{g}_x,$$
(34)

$$2St_n d\hat{v}_{1,y}/d\hat{t} = -\hat{F}_{12,n} \sin \theta_{12} - \hat{F}_{12,t} \cos \theta_{12} - \hat{F}_{13,n} \sin \theta_{13} - \hat{F}_{13,t} \cos \theta_{13} + \hat{g}_{y},$$
(35)

$$d\hat{x}_1/d\hat{t} = \hat{v}_{1,x}, \quad d\hat{y}_1/d\hat{t} = \hat{v}_{1,y},$$
 (36)

where $\hat{\mathbf{g}} = 2m\delta_{12}\mathbf{g}/(6\pi\mu a^2v_{n,0})$, $\hat{t} = v_{n,0}t/\delta_{12}$, $\hat{\mathbf{x}} = \mathbf{x}/\delta_{12}$, and $\hat{v} = \mathbf{v}/v_{n,0}$. Once the x and y coordinates of sphere 1 are known at a given time, it is relatively straightforward to determine the x and y components of spheres 2 and 3,

$$\hat{x}_2 = \hat{x}_1 + (\hat{r}_{12}/\hat{h}_a)\cos\theta_{12}, \quad \hat{y}_2 = \hat{y}_1 + (\hat{r}_{12}/\hat{h}_a)\sin\theta_{12}, \quad (37)$$

$$\hat{x}_3 = \hat{x}_2 + (\hat{r}_{23}/\hat{h}_a)\cos\theta_{23}, \quad \hat{y}_3 = \hat{y}_2 + (\hat{r}_{23}/\hat{h}_a)\sin\theta_{23},$$
 (38)

where $\hat{r}_{ij} = (4a + h_{ij})/4a$ and $\hat{h}_a = \delta_{12}/4a$, as before. To follow the rotational motion of individual particles, (15) in nondimensional form yields

$$2St_n d\hat{\omega}_1 / d\hat{t} = -5(\hat{F}_{12,t} + \hat{F}_{13,t})\cot \beta.$$
 (39)

Then, the remaining rotational velocities are found using $\hat{\omega}_{12} = \hat{\omega}_1 + \hat{\omega}_2$ and $\hat{\omega}_{23} = \hat{\omega}_2 + \hat{\omega}_3$.

IV. RESULTS AND DISCUSSION

Even for the special case of three equal spheres, with two of them initially at rest and assuming hard-sphere vs soft-sphere solid-like contacts, there are several dimensionless parameters on which the collision outcome depends, as summarized in Table I. The typical ranges of parameter values listed are based on spheres of density $\rho_s = 2\,\mathrm{g/cm^3}$ and diameter $2a_i = 4a = 0.1{-}1.0\,\mathrm{cm}$, initial normal relative velocities $v_{n,0} = 10{-}150\,\mathrm{cm/s}$, a viscous fluid of viscosity $\mu = 10\,\mathrm{g/cm} - \mathrm{s}$ and surface tension $\sigma = 20\,\mathrm{dyne/cm}$, combined thickness $\delta_{12} = \delta_1 + \delta_2 = 20{-}200\,\mu\mathrm{m}$, and minimum separation $h_{\mathrm{min}} = 0.2{-}4\,\mu\mathrm{m}$ [for typical hydrodynamic surface roughnesses, see Smart and Leighton Jr., (1989); Joseph *et al.* (2001)]. These conditions might correspond to fertilizer pellets covered with a viscous polymer, for example, whereas particles wetted with water would need smaller diameters and thinner films to give similar Stokes and capillary numbers.

The range of Stokes numbers from small to large indicates a rich variety of expected outcomes from full agglomeration (FA) to full separation (FS) post collision, as observed in experiments for colinear collisions (Donahue et al., 2010). The large values of the capillary number indicates that capillary forces are typically weak for energetic collisions, as also found previously (Donahue et al., 2010; Punch et al., 2023), though slower collisions with low-viscosity liquid coatings could exhibit important capillary effects (Darabi et al., 2009; Müller and Huang, 2016; and Buck and Heinrich, 2019). The large number of parameters would make a full mapping of the outcomes for threesphere collisions too long for the current work. Instead, we present in what follows the primary effects of varying the Stokes number, capillary number, impact angle, film thickness, and solid-contact parameters to demonstrate the different outcomes. Unless noted otherwise, these simulations use $e_{dry} = 1$ (no solid–solid losses), $\mu_f = 0$ (negligible contact friction), $\theta_{23,0} = 0$ (initially horizontal 2-3 pair), $d_{23} = d_{13}$ = 1 (equal combined film thicknesses for all pairs), and $\hat{h}_{23,0} = 1$ (2–3 and 1-2 initial separations the same). Also, without loss of generality, we specify $\alpha = 0$ (impact velocity of striker sphere oriented along the x-axis) and then vary $\theta_{12,0}$ (the initial impact angle of the 1–2 pair), with the option to also vary $\theta_{23,0}$. Finally, \hat{h}_m (dimensionless minimum surface separation) is treated as an input parameter, such as would be the case if surface roughness governed the minimum separation. For the other two mechanisms (glass transition and elastohydrodynamic

TABLE I. Dimensionless parameter definitions and typical ranges.

Parameter	Definition	Description	Range
St_n	$mv_{n,0}/6\pi\mu a^2$	Stokes number, ratio of particle inertia to viscous resistance	0.1–20
Ca	$3\mu v_{n,0}/\sigma\delta_{12}$	Capillary number ratio of viscous forces to interfacial tension	$20-3 \times 10^4$
\hat{h}_a	$\delta_{12}/4a$	Ratio of combined film thickness to sphere diameter	0.002 - 0.2
\hat{h}_m	$h_{ m min}/\delta_{12}$	Ratio of minimum separation to combined film thickness	0.001 - 0.2
$-\beta$	$\theta_{12,0}-\alpha$	Impact angle between line of centers and initial velocity	0–90°
\hat{d}_{23}	$(\delta_2 + \delta_3)/(\delta_1 + \delta_2)$	Ratio of film thickness for the 2–3 pair and 1–2 pair	0.01 - 100
$\hat{h}_{23,0}$	$h_{23.0}/(\delta_1 + \delta_2)$	Ratio of initial separation of 2–3 pair and 1–2 pair	0.01 – ∞
θ_{23}^0	$\tan^{-1}\left(\frac{y_{3,0}-y_{2,0}}{x_{3,0}-x_{2,0}}\right)$	Initial angle of the 2–3 line-of-centers from horizontal	$-120^{\circ}-120^{\circ}$
e_{dry}	$-v_{ij,n}^a/v_{ij,n}^b$	Dry coefficient of restitution	0.5-1
μ_f	$ I_{ij,t}/I_{ij,n} $	Friction coefficient for solid contact	0-0.2

deformation), the minimum separation would be an output variable that depended on the relative normal velocity and hence the Stokes number.

A. Effect of the Stokes number

Figure 5 shows snapshots of the locations of the three spheres at different times for a progression of Stokes numbers. Here, $t^* = v_{1,0}t/4a$ is a dimensionless time based on the particle diameter (instead of film thickness) and magnitude of the impact velocity (instead of the normal component of the impact velocity). For low Stokes numbers, $St_n = mv_{n,0}/(6\pi\mu a^2) = 2$, which corresponds to a low impact velocity, high fluid viscosity, and/or small particles, the collision does not have enough inertia to overcome the viscous dissipation in the fluid film, and the three particles remain fully agglomerated (FA) after the collision. For the intermediate value, $St_n = 5$, sphere 1

has enough inertia to penetrate the fluid film and contact sphere 2, then rebound through the fluid layer and separate. However, spheres 2 and 3 remain together, so the outcome is partial agglomeration (PA). For a higher value, $St_n = 10$, full separation (FS) of all three spheres occurs. These three outcomes are analogous to the experimental observations of Donahue et al. (2010) and Danczyk et al. (2022) for rectilinear collisions of three wet spheres on pendulum strings, for which they observed full agglomeration at small Stokes number, full separation at large Stokes number, and reverse Newton's cradle (in which the first sphere separates while the 2-3 pair sticks together) at intermediate separations. A fourth possibility (Newton's cradle, in which the 1-2 pair agglomerates and sphere 3 separates) was also observed in these rectilinear experiments, with appropriate choice of initial separations. As will be shown later, oblique collisions allow for the full range of PA outcomes, where sphere 1, 2, or 3 separates while the remaining two spheres agglomerate.

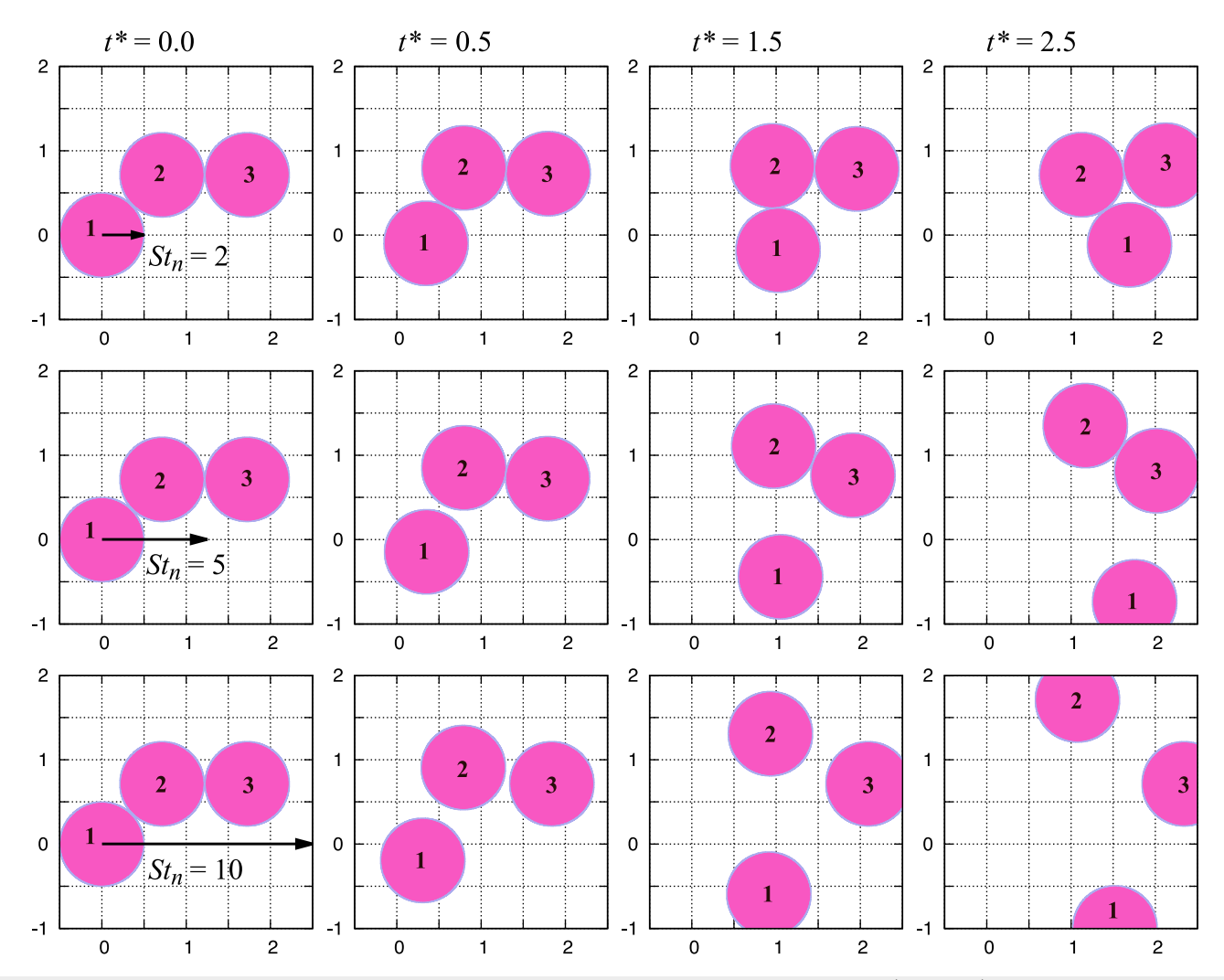


FIG. 5. Collision progression for three spheres with $St_n = 2$ (top row), 5 (middle row), and 10 (bottom row), with $\theta_{12}^0 = 45^\circ$, $\hat{h}_a = 0.01$, $\hat{h}_m = 0.05$, and negligible capillary forces

Figure 6 shows the wet coefficients of restitution for the 1–2 pair and the 2–3 pair vs the Stokes number for the conditions of Fig. 5. For an oblique collision, we followed the approach of Davis and Sitison (2020) and Donahue *et al.* (2012) to define the wet coefficient of restitution as the ratio of the normal component of the relative velocity at separation to the normal component of the impact velocity

$$e_{ij,w} = |\hat{v}_{ij,n}^s| = -v_{ij,n}^s/v_{n,0},$$
 (40)

where the superscript s refers to the moment during rebound of the i-j-pair that their fluid layers no longer overlap, even if the pair has translated or rotated a significant distance from its initial position. Equation (40) applies to both the 1–2 pair and 2–3 pair, with $v_{n,0} = v_{1,0}\cos\beta$ the normal component of the velocity of impact of sphere 1 with sphere 2 in both cases (as the initial relative velocity of spheres 2 and 3 is zero). As seen in Fig. 6, the wet coefficient of restitution for the 1–2 pair is very small for $St_n \lesssim 5$ and then rapidly increases for $St_n > 5$ as the particle inertia is relatively strong, and viscous dampening is weaker. For the 2–3 pair, the wet coefficient of restitution is small for $St_n \lesssim 8$ and increases for more vigorous collisions. The 1–2 coefficient shows a plateau and a jump in its value with increasing Stokes number, due to the interplay between the 1–2 separation and the 2–3 impact, as explained in Sec. IV C.

Shown as a short-dashed curve in Fig. 6 is the wet coefficient of restitution for a head-on, two-sphere collision under similar conditions. From Davis and Sitison (2020), it is given by

$$e_{wet} = 0$$
, $St_n < St_s$; $e_{wet} = e_{dry}(1 - St_s/St_n)$, $St_n > St_s$, (41)

where St_s is a critical value for rebound

$$St_s = \left[(1 + e_{dry})/e_{dry} \right] \left[\ln(1/\hat{h}_m) - 3\ln(2 - \hat{h}_m) + 2 - 2/(2 - \hat{h}_m) \right]. \tag{42}$$

Also shown as small circles, are simulations for an oblique, two-sphere collisions, with the stick-rotate-separate mechanism for $St_n \lesssim 4$ and

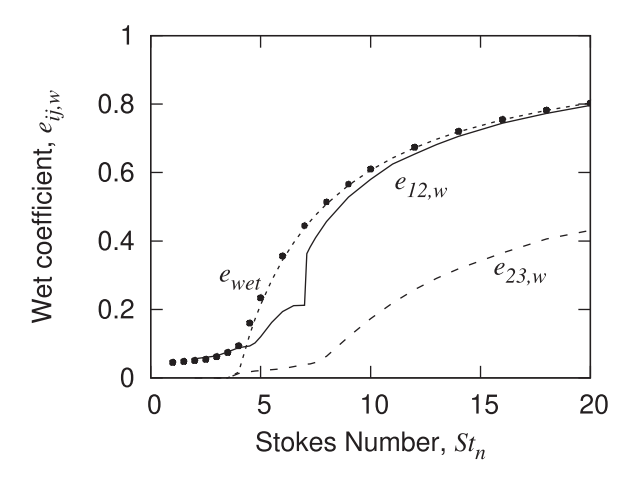


FIG. 6. Wet coefficient of restitution of the 1–2 (solid curve) and 2–3 (long: dashed curve) pairs vs Stokes number for the conditions of Fig. 5. The short-dashed curve is for a two-sphere, head-on collision using (41) and (42), whereas the small circles are for a two-sphere oblique collision under the same conditions as the three-sphere collision.

the rapid-bounce mechanism for larger Stokes numbers. For intermediate Stokes numbers, the wet coefficient of restitution is higher for the two-sphere collision than for the three-sphere collision, as the presence of the third sphere inhibits the separation of the remaining pair.

Even for small Stokes numbers, the 1-2 pair has a non-zero wet coefficient of restitution. In these cases, the rebound is not due to solid-solid contact and bouncing but rather due to centrifugal forces pulling the rotating 1-2 pair apart, similar to the results seen previously (Donahue et al., 2012; Davis and Sitison, 2020; and Punch et al., 2023) for oblique collisions of two wetted spheres. This point is illustrated in Fig. 7, where the separation of the 1-2 pair is plotted vs time for several values of the Stokes number. For large Stokes numbers ($St_n \gtrsim 5$), the striker sphere rapidly penetrates through the liquid film and impacts the target sphere and then rebounds back through the liquid film, which is referred to as "rapid bounce." For smaller Stokes numbers, the striker sphere has less inertia and is not able to bounce out of the liquid layer-indeed, for $St_n < 2.4$, it does not even reach solid contact with the target sphere. Instead, the pair sticks together due to viscous forces, undergoes rotation along with the third sphere in the agglomerated state, and then slowly separates due to centrifugal forces pulling the spheres apart. This case is referred to as "stickrotate-separate." The rapid-bounce case for $St_n = 10$ is illustrated in the bottom row of Fig. 5, whereas the stick-rotate-separate case is illustrated for $St_n = 5$ in the middle row of Fig. 5. Eventual separation due to centrifugal forces occurs even for $St_n = 2$ when there are no capillary forces to hold the spheres together, but it takes until $\hat{t} = v_{n,0}t/\delta_{12} = 183$, which corresponds to $t^* = v_{1,0}t/4a = 2.59$ and so is just beyond the last frame of Fig. 5. Also shown in Fig. 7 is the angle that the line-of-centers for the 1-2 pair makes with the horizontal, which increases from $\pi/4$ to nearly $3\pi/4$ by the time separation occurs for $St_n = 2$. In contrast, there is very little rotation of the 2–3 pair and so it remains agglomerated (Fig. 5).

B. Effect of capillary number

Although capillary forces are expected to be relatively small for the conditions of Table I with highly viscous films, their effects may be important in promoting agglomeration for less viscous films and smaller particles. To illustrate this possibility, Fig. 8 shows the

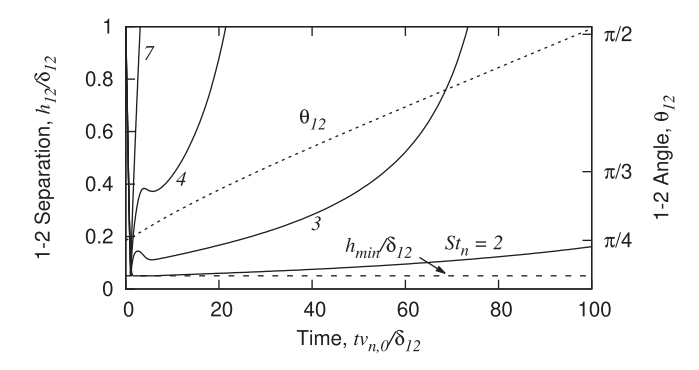


FIG. 7. Separation gap for the 1–2 pair vs time for oblique collisions with the conditions of Fig. 5 and $St_n=2$, 3, 4, and 7 (right to left). The short-dashed line is the angle of the line-of-centers of the 1–2 pair with respect to horizontal for $St_n=2$, whereas the long-dashed line shows the minimum separation where rebound occurs.

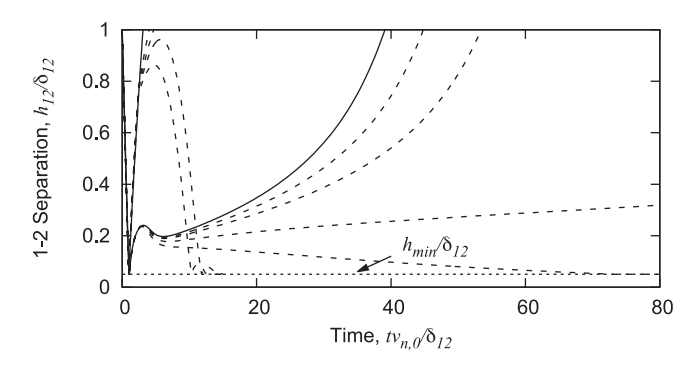


FIG. 8. Separation gap for the 1–2 pair vs time for oblique collisions with the conditions of Fig. 5 but with varying capillary numbers. The curves on the right are for $St_n=3.5$ and those on the left are for $St_n=7$. The solid curves are for $Ca\to\infty$, while the long-dashed curves are for Ca=6, 7, 8, and 10 (right to left) for $St_n=7$ and for Ca=100, 200, 500, and 1000 (right to left) for $St_n=3.5$. The short-dashed curve is for solid contact.

separation gap of the 1-2 pair for the conditions of Fig. 5 but with varying Ca at low $(St_n = 3.5)$ and moderate $(St_n = 7)$ Stokes numbers. For the larger St_n , there is rapid bounce for large Ca, and the effects of capillary forces are negligible until $Ca \lesssim 40$. In this latter range, $4/Ca \ge 0.1$, so the capillary suction forces in (27) and (28) begin to become comparable to the viscous lubrication forces and slow the rebound. Indeed, for $Ca \leq 6$, the rebound of the 1-2 pair is completely arrested and full agglomeration (FA) vs partial agglomeration (PA) occurs. For yet higher Stokes numbers, however, even smaller capillary numbers would be required to prevent rapid bouncing. The situation is quite different for smaller Stokes numbers. For $St_n = 3.5$, a slow stick-rotate-separate outcome is observed in the absence of capillary forces. However, there is noticeable slowing of the separation for Ca = 1000 and complete arrest of any separation for Ca = 100. The reason for this strong effect of capillary suction even for $Ca \gg 1$ is that the timescale for small St_n during stick-rotate behavior is the long timescale (t_L) associated with rotation instead of the short timescale (t_S) associated with penetration through the liquid film, allowing more time for capillary suction to work. Mathematically, the inertia terms on the left-hand-side of (20) and (23) become small at the long timescale and the 4/Ca capillary term on the right-hand-side of (27) and (28) then must only balance the centrifugal terms on the right-hand-sides of (20) and (23), respectively, which are proportional to $h_a = \delta_{12}/4a$ and, hence, small.

Figure 9 shows the effect of capillary number on the wet coefficient of restitution, for both the 1–2 and 2–3 pairs. It is seen that even a relatively small capillary force (Ca=100, recalling that the ratio of capillary and viscous forces is inversely proportional to Ca) is enough to eliminate the slow stick-rotate-separate outcome for the 1–2 pair at $St_n \lesssim 5$, leading to the FA outcome. The range of Stokes numbers for which the 2–3 pair remains intact is expanded to $St_n \lesssim 10$, making it more difficult to achieve the FS outcome. As Ca is decreased further, the wet coefficients of restitution are reduced for both the 1–2 pair and the 2–3 pair, due to the increased capillary suction holding them together. However, even for moderate capillary forces (Ca=10), the capillary suction has negligible effect on the wet coefficient of restitution for rapid bouncing at sufficiently high Stokes numbers.

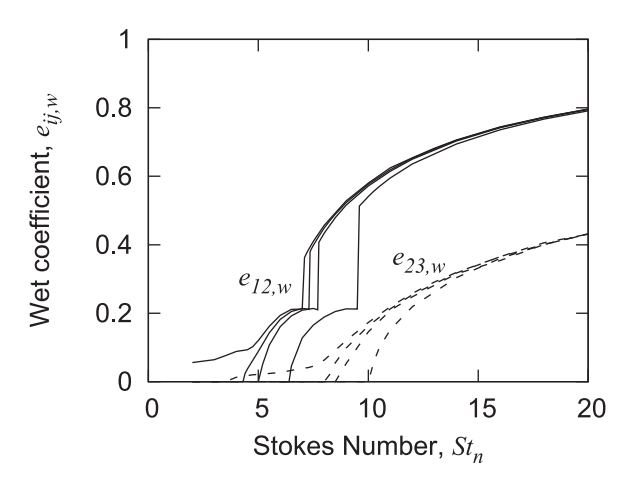
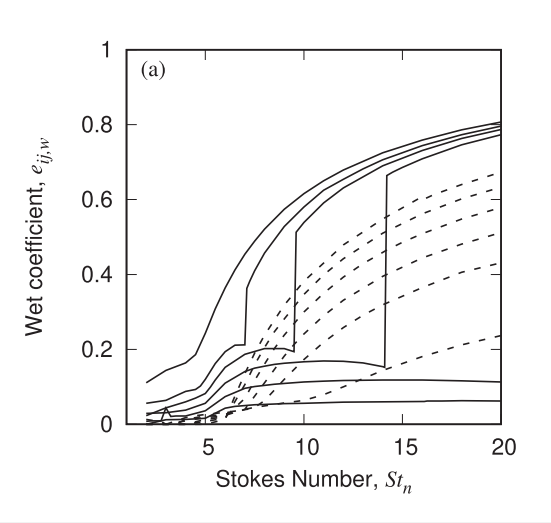


FIG. 9. Wet coefficients of restitution vs Stokes number for the conditions of Fig. 5 but with $Ca = 10, 40, 100, \text{ and } \infty$ (bottom to top or right to left).

C. Effect of impact angle

The results presented until this point in the paper are for a collision angle of 45°. Figure 10(a) shows the effects of varying the collision angle on the wet coefficients of restitution. The results indicate a rich variety of physics. For colinear collisions ($\theta_{12,0}=0$) under these conditions, the 1-2 pair always sticks together, while the 2-3 pair also remains agglomerated for Stokes numbers below a critical value of $St_n \approx 4.8$ (FA), but sphere 3 separates from the 1–2 pair for larger values of St_n , as viscous forces are then insufficient to overcome the collision inertia (PA)—see Fig. 5 of Davis (2019). This behavior is reminiscent of a Newton's cradle for dry spheres, except that the restitution coefficient for the departing sphere is reduced by viscous losses in the wet case. It is in contrast to the findings for $\theta_{12,0} > 0$, in which PA is observed at small Stokes numbers but with sphere 1 departing from the 2-3 pair by the stick-rotate-separate mechanism that is absent for colinear collisions (Donahue et al., 2010; Davis, 2019). For $\theta_{12,0} = 15^{\circ}$ and 22.5°, the wet coefficient of restitution of the 1–2 pair remains small but nonzero as the Stokes number increases, while for $\theta_{12,0} = 60^{\circ}$ it increases rapidly with increasing Stokes number beyond $St_n \approx 4$ (approaching e_{dry} as $St_n \rightarrow \infty$). The difference is due to the presence of sphere 3, as such behavior is not seen for two-sphere collisions (Davis and Sitison, 2020). For $\theta_{12,0} = 15^{\circ}$ and 22.5°, the 1–2 pair makes solid contact at high St_n and begins to bounce apart. However, before the 1-2 pair fully separates, the 2-3 pair makes contact, which slows the 1-2 rebound—see (A6). In contrast, for $\theta_{12,0}=60^{\circ}$, the 2–3 pair does not make contact until after the 1–2 pair has separated, so this slowing mechanism only occurs after the point at which $e_{12,w}$ is determined. Finally, $\theta_{12,0}=30^{\circ}$, 37.5° , and 45° represent intermediate cases. The 2-3 contact occurs before the 1-2 pair separates for $\theta_{12.0} = 30^{\circ}$ and $St_n \leq 14.1$, causing $e_{12.w}$ to remain small. For $St_n \gtrsim 14.1$, the 2-3 contact occurs after the 1-2 separation, so there is a jump in $e_{12,w}$. For $\theta_{12,0}=45^{\circ}$, the jump is smaller and occurs at $St_n \approx 7.0$.

Figure 10(b) is a contour plot for the wet coefficients of restitution. In general, both coefficients increase with increasing Stokes number at fixed impact angle. A small exception is the loop in $e_{12,w}$ near $\theta_{12,0}=35-40^{\circ}$ and $St_n=6-8$, which corresponds to the region near



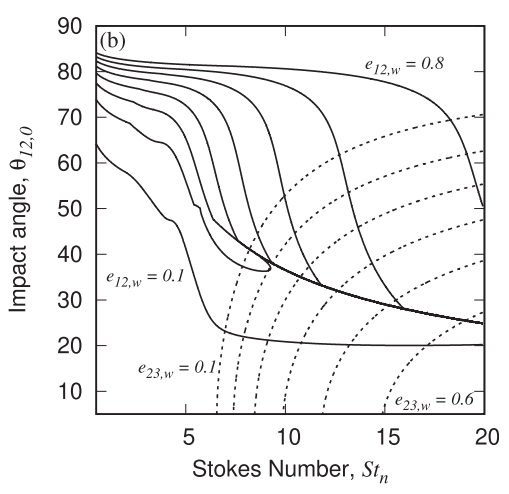


FIG. 10. (a) Wet coefficients of restitution vs Stokes numbers for the conditions of Fig. 5 but with $\theta_{12,0} = 15^{\circ}, 22.5^{\circ}, 30^{\circ}, 37.5^{\circ}, 45^{\circ}$, and 60° (bottom to top for $e_{12,w}$ and top to bottom for $e_{23,w}$). The solid curves are $e_{12,w}$ and the dashed curves are $e_{23,w}$. (b) Contour plot of the wet coefficients vs impact angle and Stokes number. The solid curves are $e_{12,w} = 0.1, 0.2, 0.3, 0.4, 0.5, 0.6, 0.7,$ and 0.8 (bottom to top) and the dashed curves are $e_{23,w} = 0.1, 0.2, 0.3, 0.4, 0.5,$ and 0.6 (top to bottom).

the local maximum in Fig. 10(a) for $\theta_{12,0}=37.5^\circ$. The confluence of curves where $e_{12,w}$ has multiple values corresponds to the jump seen in Fig. 10(a) due to 1–2 separation moving from after to before 2–3 contact. The additional data for $0.5 \le St_n \le 2$ in the upper left-hand corner of Fig. 10(b) represent the stick-rotate-separate mechanism, where the striker sphere 1 has relatively small inertia and penetrates only partway into the film separating it from the target sphere 2, and then slowly separates from the 2–3 agglomerate due to centrifugal forces. It is interesting to note that $e_{12,w}$ generally increases with increasing impact angle, as centrifugal forces are then larger and the presence of sphere 3 has less effect. However, the opposite trend is seen for $e_{23,w}$, as a smaller impact angle will more directly transfer momentum from sphere 1 to sphere 2 and then to sphere 3.

Figure 11 shows the 1–2 separation and the 2–3 separation vs time for an impact angle of 30° and several Stokes numbers. For $St_n = 7$, the 1–2 pair makes solid contact $(\hat{h}_{12} = \hat{h}_m)$ at $\hat{t} = 1.00$ and initially experiences a strong rebound. At $\hat{t} = 2.60$, however, the 2–3

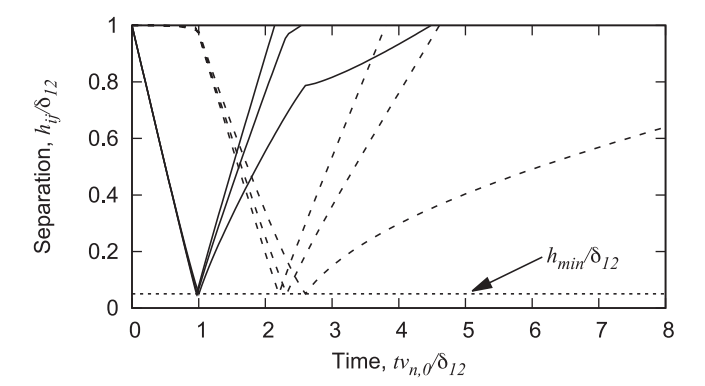


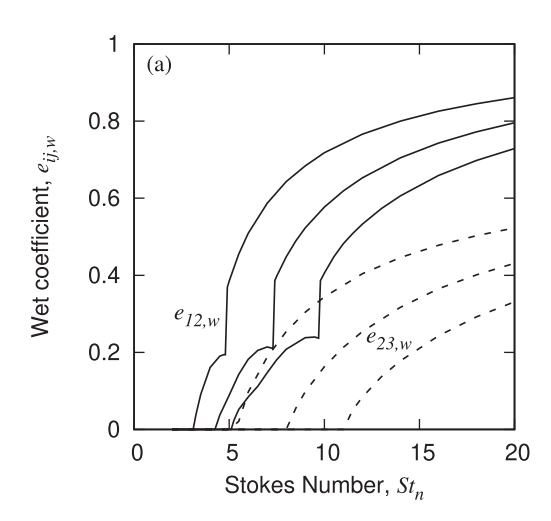
FIG. 11. Separation vs time for the 1–2 pair (solid curves) and the 2–3 pair (long-dashed curves) for $\theta_{12,0}=30^\circ$ and $St_n=7$, 12, and 20 (right to left). The rest of the conditions are the same as in Fig. 5. The short-dashed curve is where solid contact occurs

pair makes solid contact, which arrests the 1–2 rebound, so that spheres 1 and 2 slowly separate due to centrifugal forces. The rebound of the 2–3 pair after contact is not strong enough to yield separation until a much later time. For $St_n = 12$, both pairs experience rapid rebound, but the 2–3 contact again occurs before the 1–2 separation, so the 1–2 wet coefficient of restitution is relatively low ($e_{12,w} = 0.168$) while the 2–3 pair has a higher wet coefficient of restitution ($e_{23,w} = 0.393$), even though it separates at a later time. In contrast, for $St_n = 20$, the 2–3 pair makes contact ($\hat{t} = 2.20$) after the 1–2 pair separates ($\hat{t} = 2.14$) and so the relative normal motion of the 1–2 pair is not impacted until after separation, and its wet coefficient of restitution is relatively large ($e_{12,w} = 0.773$, $e_{23,w} = 0.579$).

D. Effect of film thickness

A thicker liquid layer will cause greater viscous dissipation and is expected to enhance agglomeration vs separation. However, varying the dimensionless 1–2 film thickness $(\hat{h}_a=\delta_{12}/4a)$ alone while keeping the ratio of minimum separation to the film thickness $(\hat{h}_m=h_{\rm min}/\delta_{12})$ fixed will have little effect, except for small Stokes number when the centrifugal terms in (20) and (22) play a dominant role during the slow stick-rotate-separate outcome. Instead, we consider the more realistic scenario where $h_{\rm min}$ is fixed and so $\hat{h}_m=h_{\rm min}/(4a\hat{h}_a)$ varies along with varying film thickness. Similarly, the capillary number $(Ca=3\mu v_{n,0}/\sigma\delta_{12}=3\mu v_{n,0}/4\sigma a\hat{h}_a)$ will vary with film thickness. In Fig. 12(a), we set $\hat{h}_m=0.01$ and Ca=1000 when $\hat{h}_a=0.01$ and then vary \hat{h}_a with fixed impact angle $\theta_{12,0}=45^\circ$. As expected, the wet coefficients of restitution are reduced for thicker liquid films, due to increased viscous resistance as the spheres in a pair move together and then apart.

Figure 12(b) shows related results when the film thickness is fixed but the minimum separation (e.g., roughness height) is varied. As expected, a smaller minimum separation gives smaller wet restitution coefficients, as there is greater viscous dissipation when more fluid is squeezed out of the thin film prior to solid-solid contact. Comparing



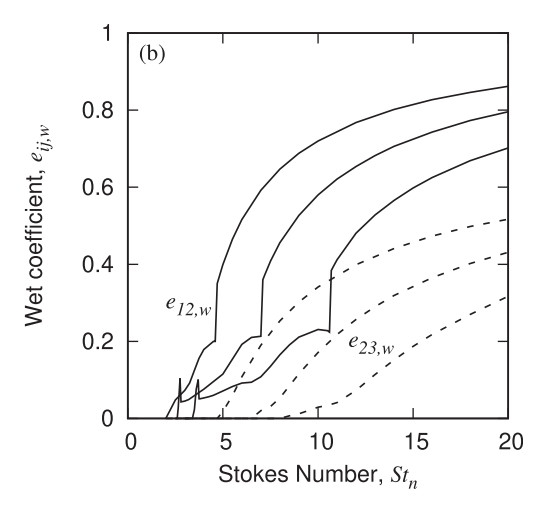


FIG. 12. (a) Wet coefficients of restitution vs Stokes number for collisions with a 45° degree impact angle and varying dimensionless film thickness $\hat{h}_a = 0.005$, 0.010, and 0.020 (top to bottom). The corresponding minimum separations are $\hat{h}_m = 0.1$, 0.05, and 0.025, and the corresponding capillary numbers are Ca = 2000, 1000, and 500, respectively. (b) Similar plot but with fixed film thickness ($\hat{h}_a = 0.01$, Ca = 1000) and varying minimum separation ($\hat{h}_m = 0.02$, 0.05 and 0.10, bottom to top).

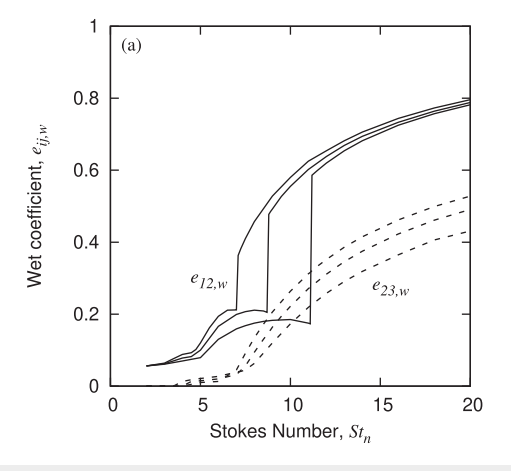
experiments to simulations like those in Fig. 12(b) could potentially provide an estimate for the effective roughness height.

E. Effect of solid-contact parameters

When the film thins such that the separation gap decreases to h_{\min} , then two parameters govern the resulting solid-solid or solid-like contact: e_{dry} and μ_f . A reduction in the dry coefficient of restitution from $e_{dry} = 1$ will reduce the wet coefficient of restitution, as seen from (41) and (42) for a head-on, two-sphere collision. Davis and Sitison (2020) showed that the contact friction gives a very slight reduction in the rotational velocity of the line-of-centers for an oblique collision of two wet spheres but has an almost negligible effect on the wet coefficient of restitution. The result for three wet spheres is quite different, as seen in Fig. 13(a). For $St_n \lesssim 4$, there is little effect of contact friction,

as either the spheres do not make contact or the contact is weak, and the separation of the 1–2 pair is due to the stick-rotate-separate mechanism. For larger St_n , the separation mechanism is rapid bouncing. Here, contact friction decreases the wet coefficient of restitution for the 1–2 pair and increases it for the 2–3 pair. With increasing friction, the separation time of the 1–2 pair is slightly delayed (due to weaker centrifugal forces) while the time at which the 2–3 pair makes solid contact is slightly decreased. As a result, 2–3 contact occurs before 1–2 separation for larger St_n with increasing friction, which suppresses the 1–2 wet coefficient of restitution while enhancing the 2–3 wet coefficient of restitution.

Figure 13(b) provides more detailed information for a threesphere collision with $St_n = 8$ under the conditions of Fig. 13(a). The 1–2 pair makes contact at $\hat{t} = 0.999$ and then bounces apart. The rotational velocity of its line-of-centers, Ω_{12} , remains at a dimensionless



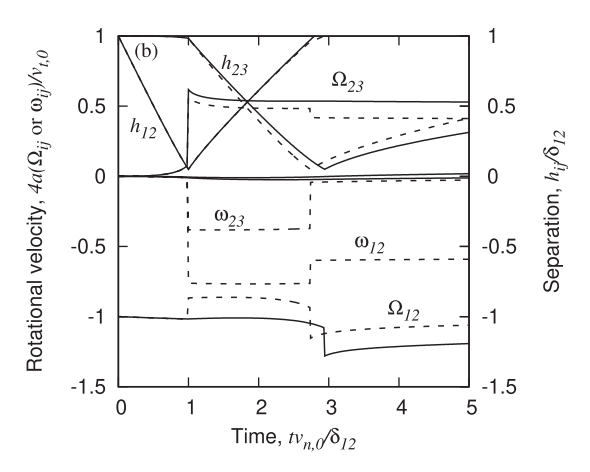


FIG. 13. (a)Wet coefficients of restitution vs Stokes number for the conditions of Fig. 5 but with contact friction coefficients of $\mu_f = 0$, 0.1 and 0.2 (left to right for $e_{12,w}$ and right to left for $e_{23,w}$). The solid curves are for the 1–2 pair, and the dashed curves are for the 2–3 pair. (b) Dimensionless rotational velocities and separation vs time for the same conditions but with $St_n = 8$ and $\mu_f = 0$ (solid curves) $\mu_f = 0.1$ (dashed curves).

value near -1 (note that Ω_{12} itself is counterclockwise and positive, but its nondimensional value is negative, due to $v_{t,0} < 0$ for $\alpha = 0$ and $\theta_{12,0}=45^\circ$) without friction ($\mu_f=0$) but experience a small jump upon contact with friction ($\mu_f = 0.1$). The rotational velocities of individual spheres ($\omega_{ij} = \omega_i + \omega_j$) remain near zero in the absence of friction but experience a jump to counterclockwise rotation with friction. In contrast, the dimensionless rotational velocity of the line-of-centers of the 2-3 pair increases slightly from zero due to viscous forces prior to contact of the 1-2 pair but then experiences a jump upon contact as momentum is transferred from sphere 1 to sphere 2, which in turn affects the relative velocity components of the 1-2 pair (see Appendix A). The normal relative velocity of the 2-3 pair also experiences a jump when the 1-2 pair makes contact, which pushes the 2-3 pair together so that it makes contact at $\hat{t} = 2.943$ (without friction) or 2.740 (with friction). When the 2-3 pair makes contact, there are additional jumps in the rotational velocities. These jumps cause small changes in the relative normal velocities of each pair during separation and, hence, in the wet coefficients of restitution. However, the large changes (jumps) in $e_{12,w}$ seen in Fig. 13(a) have a more subtle origin, as discussed above. Namely, separation of the 1-2 pair occurs at $\hat{t}=2.795$ (without friction) and $\hat{t}=2.936$ (with friction). Thus, without friction, the 1-2 separation occurs before the 2-3 contact, so $e_{12,w}$ is unaffected by the 2-3 contact and has a relatively high value ($e_{12,w} = 0.457$). In contrast, with friction, the 1-2 separation occurs after the 2-3 contact, and the wet restitution coefficient is reduced $(e_{12,w} = 0.211)$ because the contact with sphere 3 slows the movement of sphere 2 away from sphere 1.

V. SUCCESSIVE COLLISIONS

In this section, the possibility of one of the spheres undergoing successive collisions involving a change of "partners" is illustrated. For example, it is apparent from the top right panel with $St_n = 2$ and $t^* = 2.5$ in Fig. 5 that the lower particle (sphere 1) first hits the middle particle (sphere 2), rotates around it, and is about to strike the particle on the right (sphere 3). A change of partners occurs, from the 1–2 pair in close contact to the 1–3 pair in close contact. While the subsequent outcome is of interest in its own right, the ability of the algorithm to

handle such a change in partners is an important step in creating a multiparticle discrete element method (DEM) in which particle-particle contacts are made and broken throughout space and time domains.

For the three-sphere case studied here, it is noted that knowing the relative positions and velocities of the 1–2 pair and 2–3 pair at any given time are sufficient to allow for calculation of this information for the 1–3 pair using geometrical considerations, as outlined in Appendix B. Once overlap of the liquid films on spheres 1 and 3 occurs, when $h_{13} < \delta_1 + \delta_3 = \delta_{13}$, then the liquid-mediated forces between the 1–3 pair, given in (29) and (32), come into play and must be included in (20)–(25), (34), (35) and (37) to describe the dynamics of sphere 1 and the 1–2 and 2–3 pairs. Alternatively, if the 1–2 pair separates, then it may be desirable to follow the 1–3 pair instead. In this case, (20)–(22) would no longer be needed (they would still hold but become redundant) and instead be replaced by the corresponding equations for the dynamics of the 1–3 pair

$$St_{n}d\hat{v}_{13,n}/d\hat{t} = -St_{n}(\tan\beta)^{2}\hat{r}_{13}\hat{\Omega}_{13}^{2} - \hat{F}_{13,n}$$

$$-\left[\hat{F}_{12,n}\cos(\theta_{13} - \theta_{12}) + \hat{F}_{12,t}\sin(\theta_{13} - \theta_{12})\right]/2$$

$$-\left[\hat{F}_{23,n}\cos(\theta_{23} - \theta_{13}) - \hat{F}_{23,t}\sin(\theta_{23} - \theta_{13})\right]/2,$$
(43)

$$\begin{split} St_n \hat{r}_{13} d\hat{\Omega}_{13} / d\hat{t} &= 2St_n \hat{h}_a \hat{v}_{13,n} \hat{\Omega}_{13} + \hat{F}_{13,t} \cot \beta \\ &- \left[\hat{F}_{12,n} \sin(\theta_{13} - \theta_{12}) \right. \\ &- \hat{F}_{12,t} \cos(\theta_{13} - \theta_{12}) \right] (\cot \beta) / 2 \\ &+ \left[\hat{F}_{23,n} \sin(\theta_{23} - \theta_{12}) \right. \\ &+ \hat{F}_{23,t} \cos(\theta_{23} - \theta_{12}) \right] (\cot \beta) / 2, \end{split} \tag{44}$$

$$St_n d\hat{\omega}_{13}/d\hat{t} = -5(\hat{F}_{13,t} + \hat{F}_{12,t}/2 + \hat{F}_{23,t}/2)\cot\beta.$$
 (45)

Figure 14 shows an example calculation where sphere 1 changes partners by initially impacting sphere 2 and then rotating around it and hitting sphere 3. The conditions are the same as the top row $(St_n=2)$ of Fig. 5. Sphere 1 makes contact with sphere 3 (via liquid-film overlap) at $t^*=v_{1,0}t/4a=2.59$, while still in contact with sphere 2.

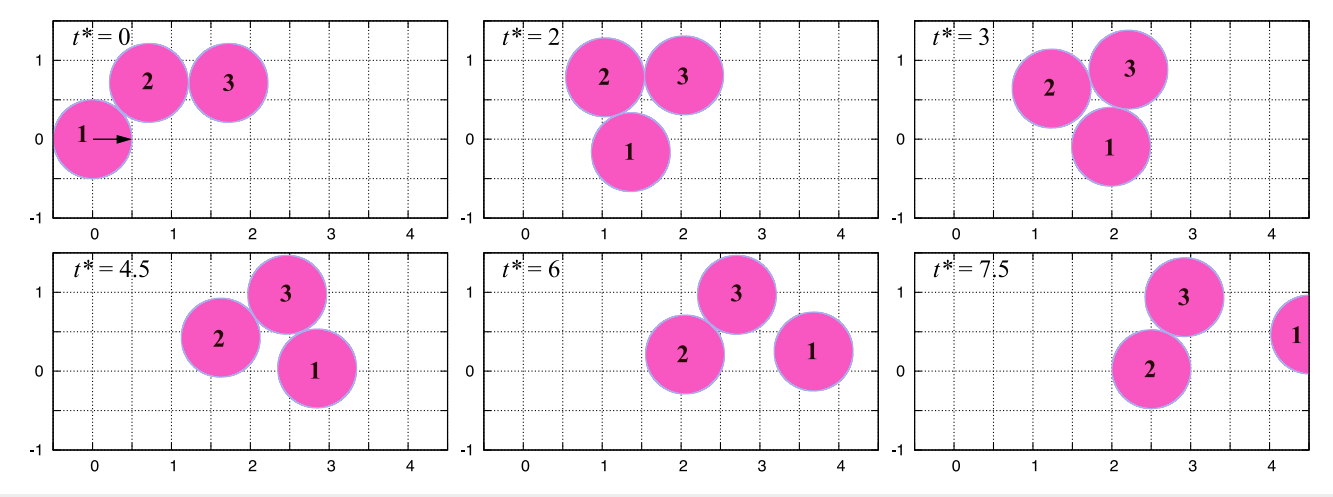


FIG. 14. Collision progression for three spheres with $St_n = 2$, $\theta_{12,0} = 45^{\circ}$, $\hat{h}_a = 0.01$, $\hat{h}_m = 0.05$, and negligible capillary forces, showing a change of partners for sphere 1 from sphere 2 to sphere 3 and then subsequent separation of the 1–3 pair.

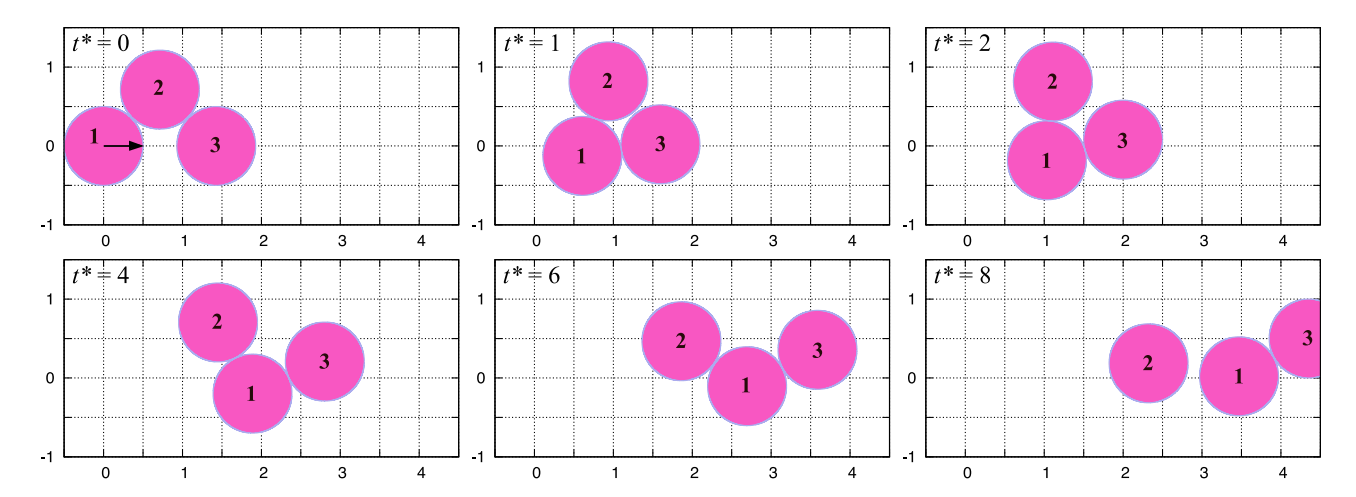


FIG. 15. Collision progress for three spheres with $St_n=2$, $\theta_{12,0}=45^\circ$, $\theta_{23,0}=-45^\circ$, $\hat{h}_a=0.01$, $\hat{h}_m=0.04$, and negligible capillary forces, showing a rearrangement on the order of the spheres and then separation of sphere 2 while the 1–3 pair remains agglomerated.

The three rotate as an agglomerated triplet for a very short time, until $t^*=2.60$, when the 1–2 pair separates. The 1–3 pair subsequently separates at $t^*=4.57$, leaving the 2–3 pair as a doublet.

In the terminology of Donahue et al. (2010), the outcome of Fig. 14 is "reverse Newton's cradle," in that the original target spheres 2 and 3 stay together while the striker sphere 1 separates after the collision. By modifying the fluid film thickness and the initial separations, Donahue et al. (2010) were also able to achieve the "Newton's cradle" outcome of sphere 3 separating and the 1-2 remaining agglomerated after the collision. For the colinear experiments and model of Donahue et al. (2010), the PA outcome of sphere 2 separating and the 1-3 pair agglomerating was not physically possible. However, for oblique collisions, the initial configuration may be modified to achieve this outcome, which is called "transfer" by Liu et al. (2017). Figure 15 shows an example where the 1-2 pair is initially oriented at a +45° angle from the x-axis, whereas the 2-3 pair is initially oriented at a -45° angle from the x-axis. Sphere 1 encounters sphere 3 at $\hat{t} = 42.7$ (t^* = 0.60). The three spheres remain joined with their centers essentially forming an equilateral triangle until $\hat{t} = 49.5$ (t* = 0.70), at which time the 2-3 pair separates. The three spheres then remain connected in a chain but with sphere 1 instead of sphere 2 in the middle until $\hat{t}=430$ (t*=6.08), at which time the 1-2 pair separates while the 1-3 pair remains agglomerated.

VI. CONCLUDING REMARKS

The dynamics of collisions of three wet spheres are examined using a microphysical discrete element method that follows the relative motion of each pair of two neighboring particles with a rotating coordinate system to track normal (along the line-of-centers) and tangential (rotation of the line-of-centers) motions. The normal and tangential lubrication forces depend on the relative particle velocity, fluid film thickness, and separation distance of the particle surfaces and are determined at each time step. When a minimum separation is reached, solid contact is assumed and treated as a hard-sphere collision with both normal (elastic) and tangential (friction) impulses.

There are rich physics with many potential outcomes for collisions of three wet spheres, including full agglomeration (FA) of all three spheres, partial agglomeration (PA) involving two spheres with the third one separating, and full separation (FS) of all three spheres, depending on the initial conditions. A key parameter is the Stokes number, representing the ratio of inertia of sphere 1 as it impacts sphere 2 to viscous forces resisting the relative normal motion. For $St_n \lesssim O(1)$, FA typically occurs, as the collision does not have enough inertia to overcome the viscous and capillary dampening forces. For $St_n > O(1)$, FS typically occurs, as the fluid forces are relatively small. For intermediate Stokes numbers, PA is typical; moreover, which sphere separates and which pair remains agglomerated can be changed by varying the initial configuration and properties. The specific Stokes numbers separating these outcomes depend on the capillary number, impact angle, and other parameters. For example, thinner films, weaker capillary forces (large Ca), and more glancing (larger impact angle) all favor separation vs agglomeration. The separation of an interacting pair of wet particles can either be a rapid-bounce separation—when the inertia is sufficiently strong for the impacting sphere to penetrate through the fluid film, make elastic solid contact with the target sphere, and rebound back through the fluid film—or a slow, stick-rotate-separate mechanism—when a pair with lower inertia initially agglomerates but then is slowly pulled apart due to centrifugal forces as it rotates. The wet coefficients of restitution are zero or very small for small Stokes numbers (due to viscous losses and capillary suction) and then increase with increasing Stokes numbers. However, their values are very sensitive to system parameters such as impact angle, film thickness, capillary number, and friction coefficient, indicating the need for accurate descriptions of wet collisions.

One potential avenue for future work is to extend the model to the scenarios when either glass transition or elastohydrodynamic deformation governs the minimum separation. The separation scales at which these mechanisms come into play depend on the relative normal velocity (Donahue *et al.*, 2010), and so the minimum separation will increase with increasing Stokes number rather than remain fixed as an input parameter. Moreover, these mechanisms occur dynamically (rather than instantly) as the lubrication pressure increases, which may require a soft-sphere vs hard-sphere approach.

The methodology described in this work can be extended to DEM simulations of many wet particles. Because the viscous and capillary forces imposed by the fluid film are decomposed into normal and tangential forces and depend on the narrow separation distance between the opposing sphere surfaces, the use of polar coordinates for particle pairs is expected to provide for highly accurate and robust simulations. In a future work, we intend to extend the method to systems of many wet particles and compare the calculations to a traditional method with Cartesian coordinates. Another key area for future study is the range of validity of the hard-sphere model for solid contact and the use of a soft-sphere model when the hard-sphere model is not valid. Finally, we hope that the rich physics predicted herein for collisions of three spheres will provide motivation for future experimental testing.

ACKNOWLEDGMENTS

This work was partially supported by NSF via Grant No. CBET-2301910. The author thanks Avery O'Neill and Gesse Roure for assisting with the manuscript and figures, and Rajarshi Chattopadhyay for also helping with the figure and manuscript as well as reviewing the equations and code.

AUTHOR DECLARATIONS

Conflict of Interest

The author has no conflicts to disclose.

Author Contributions

Robert H. Davis: Conceptualization (lead); Data curation (lead); Formal analysis (lead); Funding acquisition (lead); Investigation (lead); Methodology (lead); Project administration (lead); Resources (lead); Software (lead); Validation (lead); Visualization (lead); Writing – original draft (lead); Writing – review & editing (lead).

DATA AVAILABILITY

The data that support the findings of this study are available from the corresponding author upon reasonable request.

APPENDIX A: SOLID CONTACT

When the normal surface-to-surface separation of an i-j pair, h_{ij} , has decreased to h_{\min} , then solid-solid or solid-like contact between sphere i and sphere j occurs. It is assumed that a nearinstantaneous, hard-sphere collision takes place, resulting in a reversal of the normal relative velocity

$$v_{ij,n}^a = -e_{dry}v_{ij,n}^b, \tag{A1}$$

where the superscripts "a" and "b" refer to just after and just before the collision, respectively, and e_{dry} is the dry coefficient of restitution for the solid spheres. For simplicity, e_{dry} is treated as a constant material property, but it could easily be specified as a function of the impact velocity.

For systems of more than two spheres, the effect of the collision on the velocity of each pair is important for determining the change in relative velocities with any neighboring spheres in close contact. Integrating the normal component of the force balance (9) for relative motion over the short duration Δt of contact yields

$$m_{ij}\left(v_{ij,n}^{a}-v_{ij,n}^{b}\right)=-\int_{\Lambda_{t}}F_{ij,n}\,dt\equiv-I_{ij,n},\tag{A2}$$

where $I_{ij,n}$ is the normal component of the impulse exerted between spheres i and j during contact. Note that the other terms in (9) drop out for $\Delta t \rightarrow 0$. Then, using (A1) yields the required impulse

$$I_{ij,n} = m_{ij}(1 + e_{dry})v_{ii,n}^{b}.$$
 (A3)

Turning now to the motion of sphere *j*,

$$\Delta v_{j,n_{ij}} \equiv \left(v_{j,n_{ij}}^a - v_{j,n_{ij}}^b\right) = I_{ij,n}/m_j,\tag{A4}$$

from the component of the contact force balance on sphere j along the line-of-centers of the i-j pair. This velocity change has components both parallel and perpendicular to the line-of-centers of the j-k pair

$$\Delta v_{j,n_{ik}} = \Delta v_{j,n_{ii}} \cos(\theta_{jk} - \theta_{ij}), \quad \Delta v_{j,t_{ik}} = \Delta v_{j,n_{ii}} \sin(\theta_{jk} - \theta_{ij}),$$
 (A5)

where a frictionless contact is assumed (i.e., no change in the velocity of sphere j in the direction normal to the i-j line-of-centers; collisions with solid friction are considered below). Since the velocity of sphere k is not immediately affected by the i-j collision, the new relative velocity components of the j-k pair due to the i-j collision/rebound are

$$v_{jk,n}^{a} = v_{jk,n}^{b} + \Delta v_{j,n_{jk}} = v_{jk,n}^{b} + (m_{ij}/m_{j})(1 + e_{dry})v_{ij,n}^{b} \cos(\theta_{jk} - \theta_{ij}),$$
(A6)

$$v_{jk,t}^{a} = v_{jk,t}^{b} + \Delta v_{j,t_{jk}} = v_{jk,t}^{b} + (m_{ij}/m_{j})(1 + e_{dry})v_{ij,n}^{b} \sin(\theta_{jk} - \theta_{ij}).$$
(A7)

For collinear collisions of three equal spheres, (A6) reduces to the result derived previously by Davis (2019).

Now consider the case where there is friction during a solid-solid or solid-like contact, resulting in a nearly instantaneous change in velocity both normal and tangential to the collision surface, as well as in the rotational velocities. Following Davis and Sitison (2020), a tangential impulse proportional to the normal impulse is assumed (valid for sliding): $I_{ij,t} = \pm \mu_f I_{ij,n}$, where μ_f is the lubricated friction coefficient at contact and the upper sign here and in what follows refers to $v^s_{ij,t} > 0$, whereas the lower sign is for $v^s_{ij,t} < 0$, where $v^s_{ij,t} = -r_{ij}\Omega^b_{ij} + a_i\omega^b_i + a_j\omega^b_j$ is the relative surface velocity at the beginning of contact. Then, the tangential component of the force balance for relative motion integrated over the brief duration of contact yields

$$m_{ij}\left(v_{ij,t}^{a}-v_{ij,t}^{b}\right)=-\int_{\Delta t}F_{ij,t}\,dt=\mp\mu_{f}I_{ij,n}.\tag{A8}$$

Using (A3) then gives the tangential relative velocity after impact

$$v_{ij,t}^a = v_{ij,t}^b + \mu_f (1 + e_{dry}) v_{ij,n}^b$$
 (A9)

The rotational velocity of the line-of-centers, $\Omega_{ij} = -v_{ij,t}/r_{ij}$, after the impact is

$$\Omega_{ij}^{a} = \Omega_{ij}^{b} \pm \frac{\mu_f (1 + e_{dry}) v_{ij,n}^{b}}{r_{ii}}, \tag{A10}$$

where $r_{ij} = a_i + a_j + h_{min}$ is the center-to-center distance at impact.

The corresponding changes in rotational velocities of the individual spheres of the colliding pair are

$$\omega_i^a = \omega_i^b \mp \mu_f a_i \left(\frac{m_{ij}}{I_i}\right) (1 + e_{dry}) v_{ij,n}^b,$$

$$\omega_j^a = \omega_j^b \mp \mu_f a_j \left(\frac{m_{ij}}{I_i}\right) (1 + e_{dry}) v_{ij,n}^b,$$
(A11)

where $m_{ij} = m_i m_j / (m_i + m_j)$ and $I_i = 2 m_i a_i^2 / 5$, as before. These results follow from integrating (17) over the short duration of contact. The rotational velocity of a neighboring sphere k not participating in the collision is unchanged: $\omega_k^a = \omega_k^b$. However, the rotational velocity of the j-k pair undergoes a jump change, found by integrating the j-k equivalent of (14) over the short collision duration

$$\begin{split} \Omega^{a}_{jk} &= \Omega^{b}_{jk} + \left(m_{ij}/m_{j} \right) (1 + e_{dry}) v^{b}_{ij,n} \\ &\times \left[\sin(\theta_{jk} - \theta_{ij}) \mp \mu_{f} \cos(\theta_{jk} - \theta_{ij}) \right] / r_{jk}. \end{split} \tag{A12}$$

Similarly, the jump in the tangential velocity of sphere j causes a jump in the relative velocity of the j–k pair both parallel and perpendicular to the line-of-centers, so (A9) is replaced by

$$\begin{split} v_{jk,n}^{a} &= v_{jk,n}^{b} + \left(m_{ij} / m_{j} \right) (1 + e_{dry}) v_{ij,n}^{b} \\ &\times \left[\cos \left(\theta_{jk} - \theta_{ij} \right) \pm \mu_{f} \sin \left(\theta_{jk} - \theta_{ij} \right) \right], \\ v_{jk,t}^{a} &= v_{jk,t}^{b} - \left(m_{ij} / m_{j} \right) (1 + e_{dry}) v_{ij,n}^{b} \\ &\times \left[\sin \left(\theta_{jk} - \theta_{ij} \right) \mp \mu_{f} \cos \left(\theta_{jk} - \theta_{ij} \right) \right], \end{split} \tag{A14}$$

as seen by integrating the j–k equivalent of (9) and (14), respectively, over the short collision duration.

1. Special case of three equal spheres

First, for a 1–2 collision, with the top sign for $\hat{v}_{12,\omega}^b \sin \beta > 0$, where $\beta = \alpha - \theta_{12,0}$,

$$\Delta \hat{v}_{12,n} = -(1 + e_{dry})\hat{v}_{12,n}^b \text{ or } \hat{v}_{12}^a = -e_{dry}\hat{v}_{12}^b,$$
 (A15)

$$\Delta \hat{\Omega}_{12} = \pm \mu_f (1 + e_{dry}) \hat{v}_{12,n}^b \cot \beta / \hat{r}_{12}, \tag{A16}$$

$$\Delta \hat{\omega}_{12} = \mp 5\mu_f (1 + e_{dry}) \hat{v}_{12}^b \cot \beta, \tag{A17}$$

$$\Delta \hat{v}_{23,n} = 0.5(1 + e_{dry})\hat{v}_{12,n}^b \left[\cos(\theta_{23} - \theta_{12}) \pm \mu_f \sin(\theta_{23} - \theta_{12})\right],\tag{A18}$$

 $\Delta \hat{\Omega}_{23} = 0.5(1 + e_{dry})\hat{v}_{12,n}^b \cot \beta \left[\sin(\theta_{23} - \theta_{12}) \mp \mu_f \cos(\theta_{23} - \theta_{12}) \right] / \hat{r}_{23}, \tag{A19}$

$$\Delta \hat{\omega}_{23} = \mp 2.5 \mu_f (1 + e_{drv}) \hat{v}_{12}^b \cot \beta, \tag{A20}$$

$$\Delta \hat{v}_{1,x} = -0.5(1 + e_{dry})\hat{v}_{12,n}^b \left[\cos \theta_{12} - \mu_f \sin \theta_{12}\right], \tag{A21}$$

$$\Delta \hat{v}_{1,y} = -0.5(1 + e_{dry})\hat{v}_{12,n}^b \left[\sin \theta_{12} - \mu_f \cos \theta_{12}\right], \tag{A22}$$

$$\Delta \hat{\omega}_1 = \mp 2.5 \mu_f (1 + e_{dry}) \hat{v}_{12,n}^b \cot \beta. \tag{A23}$$

Second, for a 2–3 collision, with the top sign for $\hat{v}_{23,n}^b \sin \beta > 0$,

$$\Delta \hat{v}_{12,n} = 0.5(1 + e_{dry})\hat{v}_{23,n}^{b} \left[\cos(\theta_{23} - \theta_{12}) \mp \mu_{f} \sin(\theta_{23} - \theta_{12})\right], \tag{A24}$$

$$\Delta\hat{\Omega}_{12} = -0.5(1 + e_{dry})\hat{v}_{23,n}^b \cot\beta[\sin(\theta_{23} - \theta_{12})]$$

$$\pm \mu_f \cos(\theta_{23} - \theta_{12})] / \hat{r}_{12},$$
 (A25)

$$\Delta \hat{\omega}_{12} = \mp 2.5 \mu_f (1 + e_{dry}) \hat{v}_{23,n}^b \cot \beta, \tag{A26}$$

$$\Delta \hat{v}_{23,n} = -(1 + e_{dry})\hat{v}_{23,n}^b \text{ or } \hat{v}_{23,n}^a = -e_{dry}\hat{v}_{23,n}^b,$$
 (A27)

$$\Delta\hat{\Omega}_{23} = \pm \mu_f (1 + e_{dry}) \hat{v}_{23,n}^b \cot \beta / \hat{r}_{23}, \tag{A28}$$

$$\Delta \hat{\omega}_{23} = \mp 5\mu_f (1 + e_{dry}) \hat{v}_{23}^b {}_{n} \cot \beta.$$
 (A29)

2. Frictional arrest of sliding

The expressions above assume that the maximum friction force is achieved, so that the colliding surfaces slide over each other. These assumptions will no longer hold for nearly head-on collisions. In this case, the sphere surfaces do not slip, requiring

$$r_{ij}\Omega^a_{ii} = a_i\omega^a_i + a_j\omega^a_i \equiv v^a_{ii,\omega}. \tag{A30}$$

Then, integrating (14) over the short duration of the impulse yields

$$m_{ij}r_{ij}\left(\Omega_{ij}^{a}-\Omega_{ij}^{b}\right)=I_{ij,t},\tag{A31}$$

and integrating (17) over the duration of the impulse yields

$$I_i I_j \left(v_{ij,\omega}^a - v_{ij,\omega}^b \right) = - \left(I_i a_j^2 + I_j a_i^2 \right) I_{ij,t}, \tag{A32}$$

where $I_{ij,t}$ is the tangential impulse. Solving (A30)–(A32) for uniform solid spheres (where $I_i = 2m_i a_i^2/5$ is the moment of inertia) gives

$$I_{ii,t} = 2m_{ii}(v_{ii,o}^b - r_{ii}\Omega_{ii}^b)/7,$$
 (A33)

$$\Omega_{ii}^{a} = 5\Omega_{ii}^{b}/7 + 2v_{ii,o}^{b}/7r_{ii},$$
 (A34)

$$v_{ii,\omega}^a = 5r_{ij}\Omega_i^b/7 + 2v_{ii,\omega}^b/7.$$
 (A35)

Of course, (A30) and (A33)–(A35) only hold if the magnitude of the tangential impulse is less than the maximum value; $|I_{ii.t}| < \mu_t I_{ii.n}$ or

$$|v_{ij,\omega}^b - r_{ij}\Omega_{ij}^b| < 7\mu_f(1 + e_{dry})v_{ij,n}^b/2.$$
 (A36)

If so, then $I_{ij,t}$ from (A33) replaces the maximum value $\mu_f(1+e_{dry})v^b_{ij,n}$ in (A8)–(A29) and all \pm and \mp symbols are replaced by + and -, respectively. If (A36) is not met, then (A8)–(A29) are unchanged.

APPENDIX B: RELATIVE POSITIONS AND VELOCITIES OF 1-3 PAIR

At any time step, the relative positions and velocities of the 1–2 and 2–3 pairs may be used to determine the relative positions and velocities of the 1–3 pair (whether or not it is in close contact) from geometry. Making use of the fixed Cartesian coordinate system, the 1–3 center-to-center distance is

$$r_{13} = ((x_{12} + x_{23})^2 + (y_{12} + y_{23})^2)^{1/2},$$
 (B1)

where $x_{ij} = r_{ij} \cos \theta_{ij}$ and $y_{ij} = r_{ij} \sin \theta_{ij}$. Thus, the angle of the 1–3 center-to-center vector with the x-axis is

$$\theta_{13} = \tan^{-1}((y_{12} + y_{23})/(x_{12} + x_{23})) = \cos^{-1}((x_{12} + x_{23})/r_{13}).$$
(B2)

The gap between their surfaces, needed in the force expressions, is

$$h_{13} = r_{13} - a_1 - a_3. (B3)$$

The relative velocity components of the 1–3 pair in Cartesian coordinates at a given time step are

$$v_{13,x} = v_{12,x} + v_{23,x}, (B4)$$

$$v_{13,y} = v_{12,y} + v_{23,y},$$
 (B5)

where $v_{ij,x} = v_{ij,n} \cos \theta_{ij} - v_{ij,t} \sin \theta_{ij}$, $v_{ij,y} = v_{ij,n} \sin \theta_{ij} + v_{ij,t} \cos \theta_{ij}$, and $v_{ij,t} = -r_{ij}\Omega_{ij}$. These velocities may be converted to the normal and tangential velocities required in the force expressions

$$v_{13,n} = v_{13,x} \cos \theta_{13} + v_{12,y} \sin \theta_{13}, \tag{B6}$$

$$v_{13,t} = -v_{13,x}\sin\theta_{13} + v_{13,y}\cos\theta_{13}.$$
 (B7)

Finally, the rotational velocities for the 1-3 pair are

$$\Omega_{13} = d\theta_{13}/dt = -v_{13,t}/r_{13},\tag{B8}$$

$$\omega_{13} = \omega_1 + \omega_3 = \omega_{23} - \omega_{12} + 2\omega_1,$$
 (B9)

where ω_1 is found from (39).

REFERENCES

- Anand, A., Curtis, J. S., Wassgren, C. R., Hancock, B. C., and Ketterhagen, W. R., "Predicting discharge dynamics of wet cohesive particles from a rectangular hopper using the discrete element method (DEM)," Chem. Eng. Sci. 64(24), 5268–5275 (2009).
- Andreotti, B., Forterre, Y., and Pouliquen, O., Granular Media: Between Fluid and Solid (Cambridge University Press, 2013).
- Barnocky, G., and Davis, R. H., "Elastohydrodynamic collision and rebound of spheres: Experimental verification," Phys. Fluids 31(6), 1324-1329 (1988)
- Barnocky, G., and Davis, R. H., "The influence of pressure-dependent density and viscosity on the elastohydrodynamic collision and rebound of two spheres," J. Fluid Mech. 209, 501–519 (1989).
- Blumenfeld, R., Edwards, S. F., and Walley, S. M., "167Physics of granular systems," in *The Oxford Handbook of Soft Condensed Matter* (Oxford University Press, 2015). ISBN: 9780199667925.
- Brady, J. F., and Bossis, G., "Stokesian dynamics," Annu. Rev. Fluid Mech. 20(1), 111–157 (1988).
- Buck, B., and Heinrich, S., "Collision dynamics of wet particles: Comparison of literature models to new experiments," Adv. Powder Technol. **30**(12), 3241–3252 (2019).
- Buck, B., Lunewski, J., Tang, Y., Deen, N. G., Kuipers, J., and Heinrich, S., "Numerical investigation of collision dynamics of wet particles via force balance," Chem. Eng. Res. Des. 132, 1143–1159 (2018).
- Buck, B., Tang, Y., Heinrich, S., Deen, N. G., and Kuipers, J., "Collision dynamics of wet solids: Rebound and rotation," Powder Technol. 316, 218–224 (2017).
- Crüger, B., Salikov, V., Heinrich, S., Antonyuk, S., Sutkar, V. S., Deen, N. G., and Kuipers, J., "Coefficient of restitution for particles impacting on wet surfaces: An improved experimental approach," Particuology 25, 1–9 (2016).
- Cundall, P. A., and Strack, O. D., "A discrete numerical model for granular assemblies," Geotechnique 29(1), 47–65 (1979).

- Danczyk, M., Punch, O., Fullard, L., Hawken, M., and Holland, D. J., "A comparison of models of linear collisions between spherical particles in the pendular regime," Powder Technol. 398, 117112 (2022).
- Darabi, P., Pougatch, K., Salcudean, M., and Grecov, D., "A novel coalescence model for binary collision of identical wet particles," Chem. Eng. Sci. **64**(8), 1868–1876 (2009)
- Davis, R. H., "Elastohydrodynamic collisions of particles," PhysicoChem. Hydrodyn. 9, 41–52 (1987).
- Davis, R. H., "Simultaneous and sequential collisions of three wetted spheres," J. Fluid Mech. 881, 983–1009 (2019).
- Davis, R. H., and Sitison, J. W., "Oblique collisions of two wetted spheres," Phys. Rev. Fluids 5(5), 054305 (2020).
- Davis, R. H., Rager, D. A., and Good, B. T., "Elastohydrodynamic rebound of spheres from coated surfaces," J. Fluid Mech. 468, 107–119 (2002).
- Davis, R. H., Serayssol, J.-M., and Hinch, E. J., "The elastohydrodynamic collision of two spheres," J. Fluid Mech. 163, 479–497 (1986).
- Donahue, C. M., Brewer, W. M., Davis, R. H., and Hrenya, C. M., "Agglomeration and de-agglomeration of rotating wet doublets," J. Fluid Mech. 708, 128–148 (2012).
- Donahue, C. M., Hrenya, C. M., and Davis, R. H., "Stokes's cradle: Newton's cradle with liquid coating," Phys. Rev. Lett. 105(3), 034501 (2010).
- Ennis, B. J., Tardos, G., and Pfeffer, R., "A microlevel-based characterization of granulation phenomena," Powder Technol. 65(1-3), 257-272 (1991).
- Gidaspow, D., Multiphase Flow and Fluidization: Continuum and Kinetic Theory Descriptions (Academic Press, 1994).
- Gollwitzer, F., Rehberg, I., Kruelle, C. A., and Huang, K., "Coefficient of restitution for wet particles," Phys. Rev. E 86(1), 011303 (2012).
- Gondret, P., Hallouin, E., Lance, M., and Petit, L., "Experiments on the motion of a solid sphere toward a wall: From viscous dissipation to elastohydrodynamic bouncing," Phys. Fluids 11(9), 2803–2805 (1999).
- Guo, Y., and Curtis, J. S., "Discrete element method simulations for complex granular flows," Annu. Rev. Fluid Mech. 47, 21–46 (2015).
- Joseph, G., and Hunt, M., "Oblique particle-wall collisions in a liquid," J. Fluid Mech. 510, 71-93 (2004).
- Joseph, G., Zenit, R., Hunt, M., and Rosenwinkel, A., "Particle-wall collisions in a viscous fluid," J. Fluid Mech. 433, 329-346 (2001).
- Kantak, A., Hrenya, C., and Davis, R., "Initial rates of aggregation for dilute, granular flows of wet particles," Phys. Fluids 21(2), 023301 (2009).
- Kantak, A. A., and Davis, R. H., "Oblique collisions and rebound of spheres from a wetted surface," J. Fluid Mech. 509, 63–81 (2004).
- Kantak, A. A., and Davis, R. H., "Elastohydrodynamic theory for wet oblique collisions," Powder Technol. 168(1), 42–52 (2006).
- Kasper, J. H., Magnanimo, V., de Jong, S. D., Beek, A., and Jarray, A., "Effect of viscosity on the avalanche dynamics and flow transition of wet granular matter," Particuology **59**, 64–75 (2021).
- Lian, G., Adams, M., and Thornton, C., "Elastohydrodynamic collisions of solid spheres," J. Fluid Mech. 311, 141–152 (1996).
- Liu, P., Kellogg, K. M., LaMarche, C. Q., and Hrenya, C. M., "Dynamics of singlet-doublet collisions of cohesive particles," Chem. Eng. J. 324, 380–391 (2017)
- Liu, P., Yang, R., and Yu, A., "DEM study of the transverse mixing of wet particles in rotating drums," Chem. Eng. Sci. 86, 99–107 (2013).
- Liu, P., Yang, R., and Yu, A., "The effect of liquids on radial segregation of granular mixtures in rotating drums," Granular Matter 15, 427–436 (2013).
- Ma, J., Liu, D., and Chen, X., "Experimental study of oblique impact between dry spheres and liquid layers," Phys. Rev. E 88(3), 033018 (2013).
- Müller, P., and Pöschel, T., "Oblique impact of frictionless spheres: On the limitations of hard sphere models for granular dynamics," Granular Matter 14, 115–120 (2012).
- Müller, T., and Huang, K., "Influence of the liquid film thickness on the coefficient of restitution for wet particles," Phys. Rev. E 93(4), 042904 (2016).
- Nedderman, R. M., Statics and Kinematics of Granular Materials (Cambridge University Press, 1992).
- Pähtz, T., Durán, O., De Klerk, D. N., Govender, I., and Trulsson, M., "Local rheology relation with variable yield stress ratio across dry, wet, dense, and dilute granular flows," Phys. Rev. Lett. 123(4), 048001 (2019).

- Punch, O., Danczyk, M., Hawken, M., and Holland, D. J., "A comparison of pendulum experiments and discrete-element simulations of oblique collisions of wet spheres," AIChE J. 69(3), e17989 (2023).
- Radl, S., Kalvoda, E., Glasser, B. J., and Khinast, J. G., "Mixing characteristics of wet granular matter in a bladed mixer," Powder Technol. 200(3), 171–189 (2010).
- Schmelzle, S., and Nirschl, H., "DEM simulations: Mixing of dry and wet granular material with different contact angles," Granular Matter 20, 1–13 (2018).
- Smart, J. R., and Leighton, Jr., D. T., "Measurement of the hydrodynamic surface roughness of noncolloidal spheres," Phys. Fluids A: Fluid Dyn. 1(1), 52–60 (1989).
- Stratton, R., and Wensrich, C., "Modelling of multiple intra-time step collisions in the hard-sphere discrete element method," Powder Technol. 199(2), 120–130 (2010).
- Sutkar, V. S., Deen, N. G., Padding, J. T., Kuipers, J., Salikov, V., Crüger, B., Antonyuk, S., and Heinrich, S., "A novel approach to determine wet restitution coefficients through a unified correlation and energy analysis," AIChE J. 61(3), 769–779 (2015).

- Tang, T., He, Y., Ren, A., and Wang, T., "Experimental study and DEM numerical simulation of dry/wet particle flow behaviors in a spouted bed," Ind. Eng. Chem. Res. 58(33), 15353–15367 (2019).
- Umer, M., and Siraj, M. S., "DEM studies of polydisperse wet granular flows," Powder Technol. 328, 309–317 (2018).
- Washino, K., Chan, E. L., Miyazaki, K., Tsuji, T., and Tanaka, T., "Time step criteria in DEM simulation of wet particles in viscosity dominant systems," Powder Technol. **302**, 100–107 (2016).
- Washino, K., Tan, H., Hounslow, M., and Salman, A., "A new capillary force model implemented in micro-scale CFD-DEM coupling for wet granulation," Chem. Eng. Sci. 93, 197–205 (2013).
- Yang, F.-L., and Hunt, M., "Dynamics of particle-particle collisions in a viscous liquid," Phys. Fluids 18(12), 121506 (2006).
- Zhang, H., and Li, S., "DEM simulation of wet granular-fluid flows in spouted beds: Numerical studies and experimental verifications," Powder Technol. 318, 337–349 (2017).